Purdue University
Purdue e-Pubs

Department of Electrical and Computer Engineering Technical Reports

Department of Electrical and Computer Engineering

5-1-1985

A Critical Analysis of the Rose-Weaver Measurement Technique for BSF Silicon Solar Cells

Edmund K. Banghart
Purdue University

Follow this and additional works at: https://docs.lib.purdue.edu/ecetr

Banghart, Edmund K., "A Critical Analysis of the Rose-Weaver Measurement Technique for BSF Silicon Solar Cells" (1985). *Department of Electrical and Computer Engineering Technical Reports.* Paper 541.
https://docs.lib.purdue.edu/ecetr/541

This document has been made available through Purdue e-Pubs, a service of the Purdue University Libraries. Please contact epubs@purdue.edu for additional information.

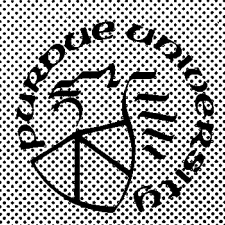

A Critical Analysis of the Rose-Weaver Measurement Technique for BSF Silicon Solar Cells

Edmund K. Banghart

TR-EE 85-6
May 1985

School of Electrical Engineering
Purdue University
West Lafayette, Indiana 47907

A CRITICAL ANALYSIS OF THE ROSE-WEAVER MEASUREMENT TECHNIQUE FOR BSF SILICON SOLAR CELLS

A Thesis

Submitted to the Faculty

of

Purdue University

by

Edmund K. Banghart

In Partial Fulfillment of the

Requirements for the Degree

of

Master of Science in Electrical Engineering

May 1985

dedicated
to my mother and father

ACKNOWLEDGMENTS

I would like to express my gratitude to my major professor, Professor Richard J. Schwartz, for his guidance, encouragement, and patience in the undertaking of this thesis. Professor Schwartz's enthusiastic nature and concern for matters beyond those of strictly an academic bearing have been a constant source of inspiration for me.

I would also like to thank Professor Jeffrey L. Gray for his helpful suggestions throughout the course of this project. Professor Gray, besides being an expert in the use of SCAP1D, is a great friend. Many times, we have discussed the adventures and misadventures of Boilermaker football and basketball.

I offer my sincere thanks, as well, to Professors James A. Cooper and William H. Hayt, Jr. for their review of this thesis and their service on my examining committee.

I am likewise indebted to the EE technical typing and illustration staff, especially Sharon Katz, Vicky Spence, Linda Stovall, and Mickey Krebs, for their skillful work in the preparation of this thesis.

Finally, I would like to thank my research group colleagues and all my friends who stood by me and helped me realize one of my dreams.

This thesis has been made possible through the support of Sandia National Laboratories, Document Number 52-5675.

TABLE OF CONTENTS

Page

APPENDICES

LIST OF TABLES

LIST OF FIGURES

ABSTRACT

Banghart, Edmund K. M.S.E.E., Purdue University. May 1985. A Critical Analysis of the Rose-Weaver Measurement Technique for BSF Silicon Solar Cells. Major Professor: Richard J. Schwartz.

The design of the optimal efficiency silicon solar cell requires the minimization of several performance-limiting phenomena. In particular, much improvement is necessary to decrease the loss of minority carriers to recombination. Thus, in order to focus our design efforts in the development of an optimal efficiency solar cell it is imperative that we be able to experimentally distinguish and assign values to the different forms of minority carrier recombination in the cell.

Recently, B. H. Rose and H. T. Weaver of Sandia National Laboratories have proposed a method to evaluate minority carrier recombination in the back surface field (BSF) solar cell through measurement of the short circuit current and open circuit voltage decay rates. In this thesis, we critically analyze the Rose-Weaver Method. In particular, we investigate the mathematical model formulated by Rose and Weaver to describe the decay of the short circuit current and the open circuit voltage.

A study of the model equations reveals that, for even small fluctuations in the experimental measurements, a large variation in the model solutions occurs. Moreover, the solution of the model is shown to rely on extremely accurate (perhaps unobtainably accurate) knowledge of material parameters.

To avoid dependence on material parameters, we analyze a second experiment in which the back surface field of the solar cell is removed. However, the

model which results from combining this experiment with the original experiment shows an even greater variation of the model solutions to uncertainty in the experimental measurements.

In summary, unless we make extremely precise measurements and avoid dependence on imprecisely known material parameters, particularly, n_i, the Rose-Weaver Method can lead to radically different descriptions of minority carrier recombination in the solar cell.

CHAPTER I
INTRODUCTION

The design of an optimal efficiency silicon solar cell requires the minimization of several performance-limiting phenomena. These phenomena include contact grid shadowing, front surface reflection, series resistance, and minority carrier recombination. Great strides have been made in reducing the first three phenomena to negligible levels. However, much improvement is still necessary to decrease the loss of minority carriers to recombination. Should the recombination in the silicon solar cell be ideally reduced, efficiencies approaching 30% under AM1.5 illumination at 300 suns, as predicted by Schwartz and Gray [1], appear feasible. This forecast represents a notable improvement over the 20% efficiency at 50 to 100 suns presently reported for the silicon solar cell [2].

Clearly, to reduce the minority carrier recombination in the silicon solar cell, we must be able to properly identify and quantify the various types of minority carrier recombination found in the device. Only then can we know where to focus our efforts in designing an optimal efficiency solar cell. Recently, B. H. Rose and H. T. Weaver of Sandia National Laboratories have proposed a technique, known as the Rose-Weaver Method [3], to experimentally distinguish and assign values to the different forms of minority carrier recombination in the back surface field (BSF) solar cell. Central to the method is the measurement of the short circuit current and open circuit voltage decay rates of the cell.

The purpose of this thesis is to critically review the Rose-Weaver Method. We will examine the assumptions made by Rose and Weaver in the development of their method. More importantly, we will attempt to provide the experimentalist with information concerning the degree of experimental accuracy required for meaningful application of the method.

We begin this chapter by presenting a review of the fundamentals of solar cell operation, using the P^+N solar cell as our example. We then discuss in detail the types of minority carrier recombination found in the P^+N solar cell. Next, by measurement of the total saturation current, we describe how we can

completely determine the recombination in the P^+N solar cell. However, when a back surface field is added to a P^+N solar cell in which the base width of the cell is comparable to the minority carrier diffusion length in the base, we observe that we can no longer determine the cell recombination completely from a measurement of the total saturation current. To properly quantify recombination in the P^+NN^+ BSF solar cell, we must make additional measurements. The Rose-Weaver Method, introduced in Chapter II, provides us with these needed measurements.

1.1 Fundamentals of Solar Cell Operation

To provide a sound basis for the analysis of minority carrier recombination in solar cells, we find it helpful to review the basic principles of solar cell operation.

Figure 1.1 illustrates a typical P^+N solar cell. A solar cell is essentially a large area semiconductor junction diode. In the figure, we show a thin, heavily doped p-type emitter region and a wider, more lightly doped n-type base region. The base and emitter regions are separated by the space-charge region at the semiconductor junction. The base region is connected to the external circuit by an ohmic contact at the back surface of the solar cell. The emitter region is also connected to the external circuit by an ohmic contact. Unlike the ohmic contact to the base which covers the entire back surface of the solar cell, the ohmic contact to the emitter covers only a small portion of the front surface. The reason for this design is to allow a maximum amount of light to enter the device. The remaining portion of the front surface is then covered with a thin, transparent layer of oxide which passivates the silicon surface.

While we have chosen to make the emitter p-type and the base n-type in the diagram, we could just as easily have made our P^+N junction with the doping types reversed. However, for the sake of consistency, we will assume for the remainder of this thesis a p-type emitter and an n-type base. With this convention, the minority carriers in the emitter are electrons and the minority carriers in the base are holes.

The solar cell is operated by attaching the cell to an external load and providing a photon excitation at the front of the device. The photons pass into the structure and are absorbed, generating electron-hole pairs in the emitter, base, and space-charge regions (Figure 1.2). By diffusion, many of the minority carriers in the emitter and in the base are likely to reach the space-charge region. The characteristic length for this diffusion, known as the diffusion

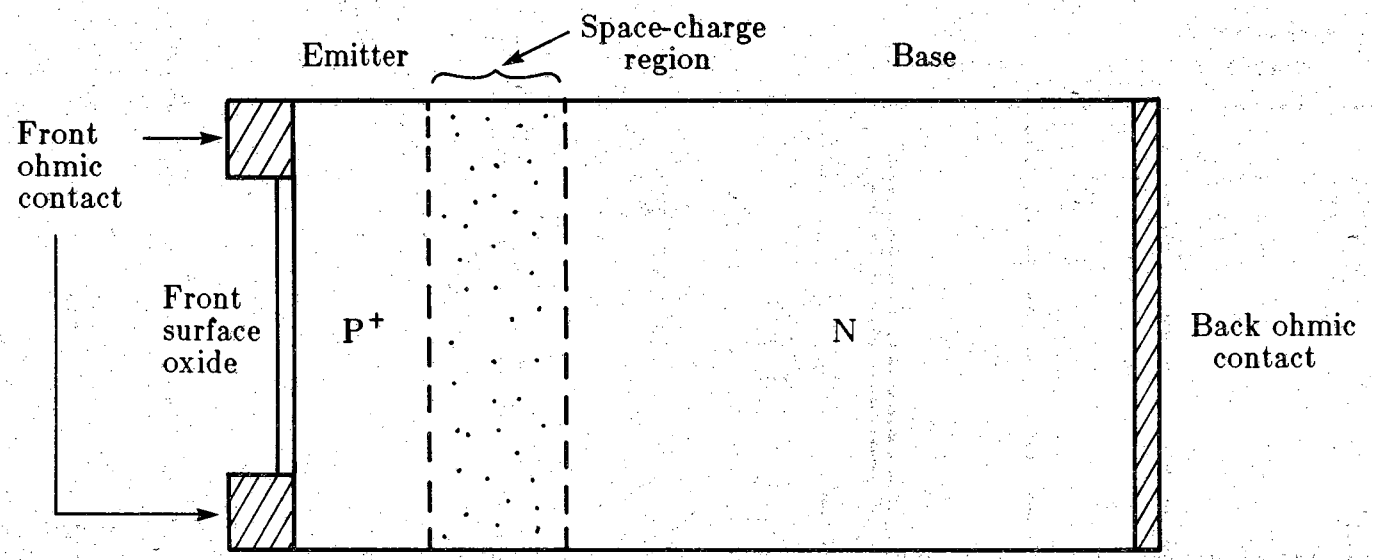

Figure 1.1 Typical P^+N Solar Cell.

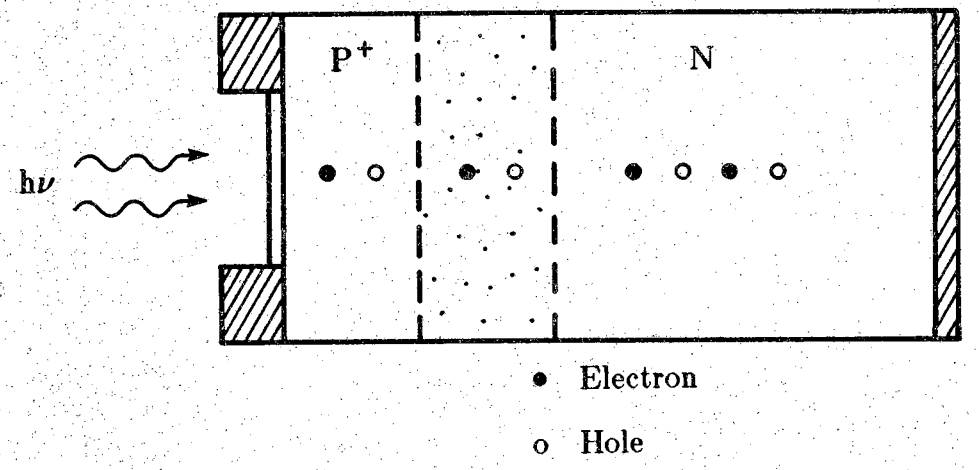

Figure 1.2 Electron-Hole Pair Generation.

length, L, is defined here as $L = \sqrt{D\tau}$, where D is the minority carrier diffusion coefficient and τ is the minority carrier lifetime. A large electric field created by the uncompensated donor and acceptor ions in the space-charge region sweeps the minority carrier holes from the base into the emitter and the minority carrier electrons from the emitter into the base (Figure 1.3). This electric field also separates the electron-hole pairs generated in the space-charge region, again sending the holes into the emitter and electrons into the base. The current produced by these light-generated carriers, I_{light}, flows in the same direction as the reverse-biased current of the P^+N junction. At the same time, the recombination of minority carriers in the solar cell, the details of which will be discussed in the following section, gives rise to the dark current, I_{dark}, which is just the forward-biased current of the P^+N junction and therefore opposes the light-generated current.

For negligible series and shunt resistance losses in the cell, we can draw the solar cell equivalent circuit as shown in Figure 1.4. In the diagram, we depict the light-generated current by a current source, the dark current by a diode, and the load by a resistance, R_{load}. The total current through the load is then simply

$$I_{load} = I_{light} - I_{dark}. \tag{1.1}$$

We typically work in terms of current density in our study of recombination and thus rewrite the above equation as

$$J_{load} = J_{light} - J_{dark}. \tag{1.2}$$

This conversion is strictly valid only when the photo-active area of the device is equal to the total area of the device. Area masked by the front contacts typically reduces the photo-active area 6-8 % below the total area of the device [4]. For a first order approximation, we will neglect this difference.

Since J_{dark} is the forward-biased current density of the P^+N junction, we can replace J_{dark} with the Shockley diode equation [5] to obtain

$$J_{load} = J_{light} - J_o \left[\exp\left(\frac{V_{load}}{n V_T} \right) - 1 \right] \tag{1.3}$$

where J_o is the total saturation current density, V_{load} is the voltage across the load, V_T is the thermal voltage, and n is the junction quality factor. The thermal voltage is defined as k_BT/q, where k_B is Boltzmann's constant, q is the electronic charge, and T is the temperature in degrees Kelvin. In SI units, $k_B = 1.38066 \times 10^{-23}$ joules per degree Kelvin and $q = 1.6 \times 10^{-19}$ coulombs.

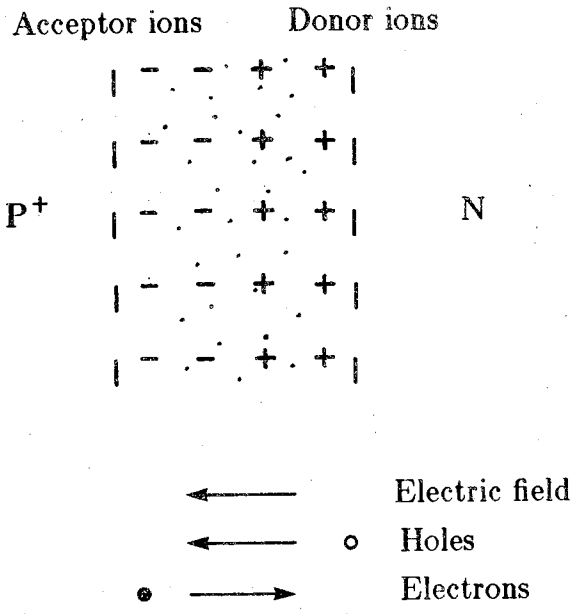

Figure 1.3 Minority Carrier Collection.

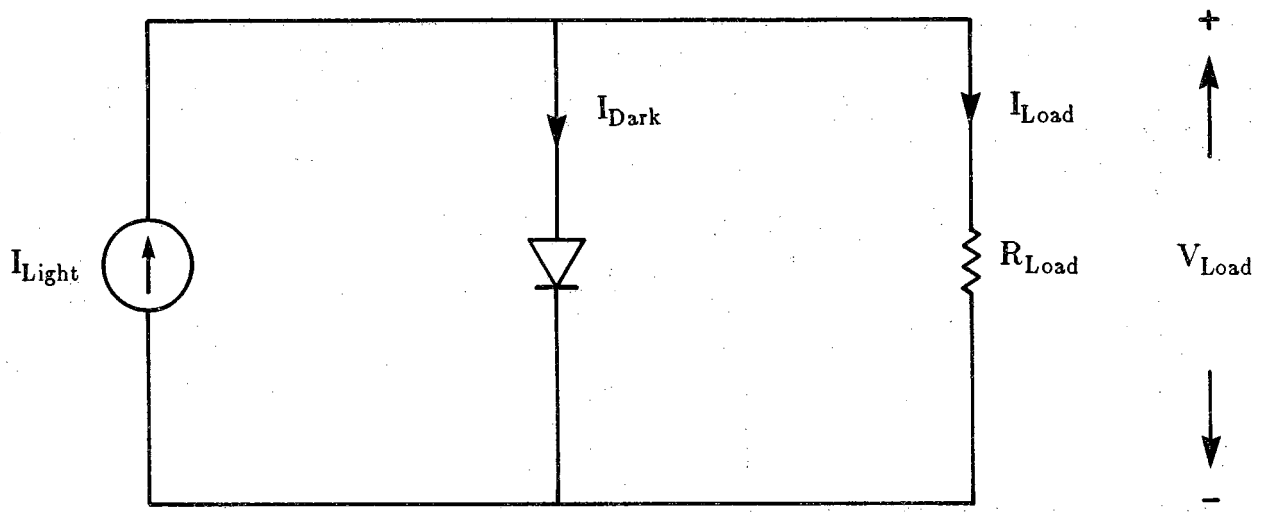

Figure 1.4 Solar Cell Equivalent Circuit.

The junction quality factor, n, will be discussed in greater detail in later sections.

Two special cases of solar cell operation are of particular interest to the device analyst. These cases are the short circuit current case and the open circuit voltage case.

To obtain the short circuit current condition, we set $R_{load} = 0$. Such action results in zero voltage across the output. That is, $V_{load} = 0$. Equation 1.3 now becomes

$$J_{sc} = J_{load} = J_{light}. \tag{1.4}$$

The second case, the open circuit voltage condition, is reached by setting $R_{load} = \infty$. This constraint renders $J_{load} = 0$. Equation 1.3 then becomes, upon rearrangement,

$$V_{oc} = V_{load} = n V_T \ln\left(\frac{J_{light}}{J_o} + 1\right). \tag{1.5}$$

But, $J_{light} = J_{sc}$ from Equation 1.4. Hence,

$$V_{oc} = n V_T \ln\left(\frac{J_{sc}}{J_o} + 1\right). \tag{1.6}$$

Rearranging Equation 1.6, we find a useful expression demonstrating the functional dependence of J_{sc} on V_{oc},

$$J_{sc} = J_o\left[\exp\left(\frac{V_{oc}}{n V_T}\right) - 1\right]. \tag{1.7}$$

Assuming $V_{oc} >> V_T$ and inferring n from the slope of a logarithmic plot of the short circuit current density versus the open circuit voltage, we can determine the total saturation current density, J_o, from the equation above. Explicitly,

$$J_o = J_{sc} \exp\left(-\frac{V_{oc}}{nV_T}\right). \tag{1.8}$$

We will find the measurement of J_o a useful starting point in determining the minority carrier recombination in solar cells.

1.2 Minority Carrier Recombination in Solar Cells

In order to minimize the minority carrier recombination in a silicon solar cell it is first necessary to understand where in the cell the photo-generated minority carriers are lost. We again take the P^+N solar cell as our basic example. We will extend our discussion to include the back surface field solar cell in the following section.

In a P^+N solar cell the loss of minority carriers to recombination occurs: (1) at the front ohmic contact, (2) at the passivated silicon surface, (3) at the back ohmic contact, (4) in the quasi-neutral base, (5) in the quasi-neutral emitter, and (6) in the space-charge region. In Figure 1.5 we indicate the six locations of minority carrier loss to recombination in the P^+N solar cell.

The front ohmic contact, formed by the deposition of metal on the heavily doped semiconductor, presents a surface at which the minority carrier electrons readily recombine. In general, we describe the recombination of minority carriers at a surface in terms of the surface recombination velocity. For the case of minority carrier electrons at a surface, the mathematical description of the recombination is [4]

$$J_n\Big|_{surface} = qS_n \Delta n_p\Big|_{surface} \tag{1.9}$$

where J_n is the minority carrier electron current at the surface, Δn_p is the excess minority carrier electron concentration at the surface, and S_n is the surface recombination velocity for the minority carrier electrons. A similar expression is written for minority carrier hole recombination at a surface,

$$J_p\Big|_{surface} = qS_p \Delta p_n\Big|_{surface}. \tag{1.10}$$

Thus, at the front ohmic contact, we use Equation 1.9 to model the recombination. In particular, we designate the surface recombination velocity for minority carrier electrons by S_{n_m}, where the subscript m refers to the metallic ohmic contact. The surface recombination velocity at an ohmic contact is quite large and approaches the thermal velocity-limited value of 5.2×10^6 cm–sec^{-1} in silicon [5].

At the silicon surface, the abrupt termination of the silicon lattice results in unsatisfied chemical bonds. Although the formation of an oxide layer over the silicon passivates most of the dangling bonds, some of the bonds remain uncovered and provide centers for minority carrier electron recombination. Again, we can describe the minority carrier electron recombination at the silicon surface in terms of the surface recombination velocity through Equation

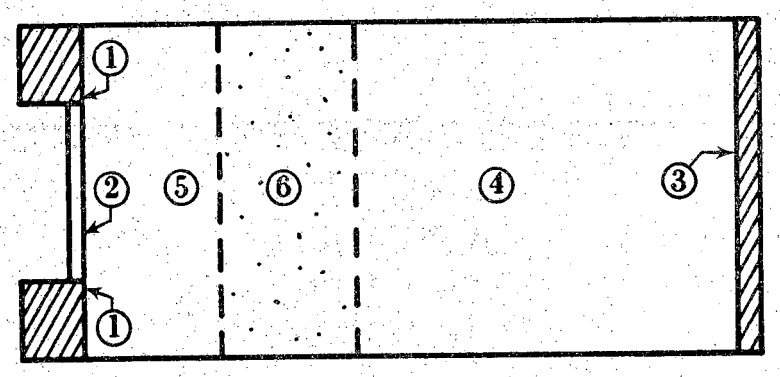

① Front ohmic contact

② Passivated silicon surface

③ Back ohmic contact

④ Quasi-neutral base

⑤ Quasi-neutral emitter

⑥ Space-charge region

Figure 1.5 Locations of Minority Carrier Recombination.

1.9. In this case, the surface recombination velocity is called S_{n_s}, where the subscript s refers to the passivated silicon surface. The surface recombination velocity at a passivated silicon surface is typically several orders of magnitude less than that found at an ohmic contact [4].

It should be noted that for one dimensional models we usually combine the electron recombination due to the front ohmic contact with that due to the passivated silicon surface. The result of this combination is an effective surface recombination velocity, $S_{n_{eff}}$, for electrons at the front surface of the cell.

At the back ohmic contact, we describe the rate of minority carrier hole recombination by means of the surface recombination velocity through Equation 1.10. In this instance, the entire back surface of the solar cell is an ohmic contact. Thus, the surface recombination velocity for holes at the back surface is just S_{p_m}, where the subscript m again refers to the metallic ohmic contact. As before, we expect S_{p_m} to approach the thermal velocity limit.

In the quasi-neutral base, recombination occurs through energy traps inside the forbidden gap produced by crystal defects in the silicon lattice. This type of recombination is known as Shockley-Hall-Read (SHR) recombination [5]. Under SHR theory for low level injection conditions, we describe the recombination in the quasi-neutral base by the minority hole lifetime, τ_p.

In the quasi-neutral emitter, Auger recombination and bandgap narrowing [5], in addition to SHR recombination, must be considered. In order to describe the recombination in the quasi-neutral emitter, we use an effective minority electron lifetime, $\tau_{n_{eff}}$.

Between the emitter and the base lies the space-charge region. Under a forward bias, the minority carriers crossing the space-charge region exceed their equilibrium values. Consequently, minority carriers recombine in the space-charge region. As in the case of the quasi-neutral base and emitter, we describe the loss of minority carriers to recombination in the space-charge region by a minority carrier lifetime, τ_{rg} [6].

In general, the six locations of minority carrier recombination in the solar cell can be associated with three recombination currents: the base, emitter, and space-charge region recombination currents. Minority carrier recombination at the back ohmic contact and in the quasi-neutral base, described by S_{p_m} and τ_p, is associated with the base recombination current, J_b. Minority carrier recombination at the front ohmic contact, at the passivated silicon surface, and in the quasi-neutral emitter, described by $S_{n_{eff}}$ and $\tau_{n_{eff}}$, is associated with the emitter recombination current, J_e. Finally, minority carrier recombination in

the space-charge region, described by τ_{rg}, is associated with the space-charge recombination current, J_{rg}. Actually, these three recombination currents are just components of the junction dark current, J_{dark}. That is,

$$J_{dark} = J_b + J_e + J_{rg}. \tag{1.11}$$

The junction dark current, we recall, is simply the forward-biased current of the P^+N junction, which opposes the photo-generated current in the solar cell. Figure 1.6 summarizes the above discussion by illustrating the contributions made by the six locations of minority carrier recombination in the solar cell to the three components of the junction dark current.

For low level injection conditions, we use the Shockley diode equation to write Equation 1.11 for the dark current as

$$J_{dark} = J_{bo}\left[\exp\left(\frac{V}{V_T}\right) - 1\right] + J_{eo}\left[\exp\left(\frac{V}{V_T}\right) - 1\right] + J_{rgo}\left[\exp\left(\frac{V}{nV_T}\right) - 1\right] \tag{1.12}$$

where J_{bo}, J_{eo}, and J_{rgo} are the saturation current densities of the base, emitter, and space-charge region, respectively. Equation 1.12 is often written inexactly [5] as

$$J_{dark} = J_o\left[\exp\left(\frac{V}{nV_T}\right) - 1\right] \tag{1.13}$$

where J_o is the total saturation current density. For voltages at which the injection current components, J_b and J_e, are dominant, $n = 1$. For lower voltages at which the space-charge recombination current component, J_{rg}, becomes significant, n is between 1 and 2. Figure 1.7 illustrates the current-voltage characteristic of the solar cell and indicates the regions in which the various current components described above are dominant. It is worth noting that for negligible series resistance the dark J-V characteristic is equivalent to the J_{sc}–V_{oc} characteristic.

In conclusion, we have one parameter, the junction dark current, which embodies all of the various forms of minority carrier recombination in the solar cell: the front and back surface recombination velocities; and the quasi-neutral base, quasi-neutral emitter, and space-charge region minority carrier lifetimes. Minimizing the junction dark current and minimizing each form of the minority carrier recombination are, then, equivalent objectives in improving the photo-performance of the solar cell.

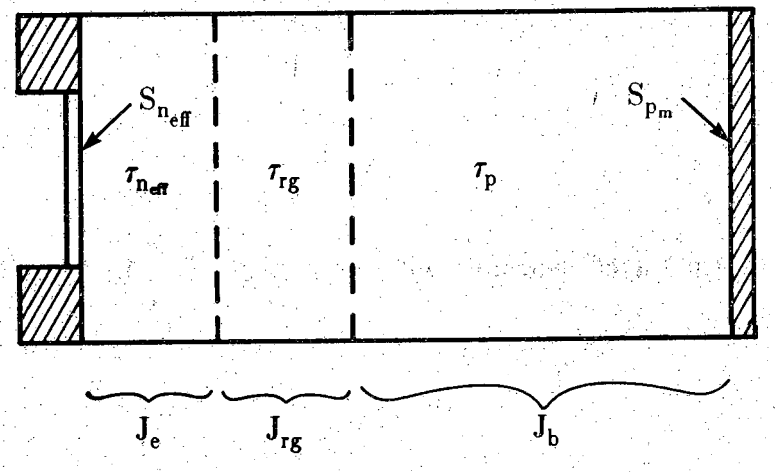

$$J_{dark} = J_e + J_{rg} + J_b$$

Figure 1.6 Components of the Junction Dark Current.

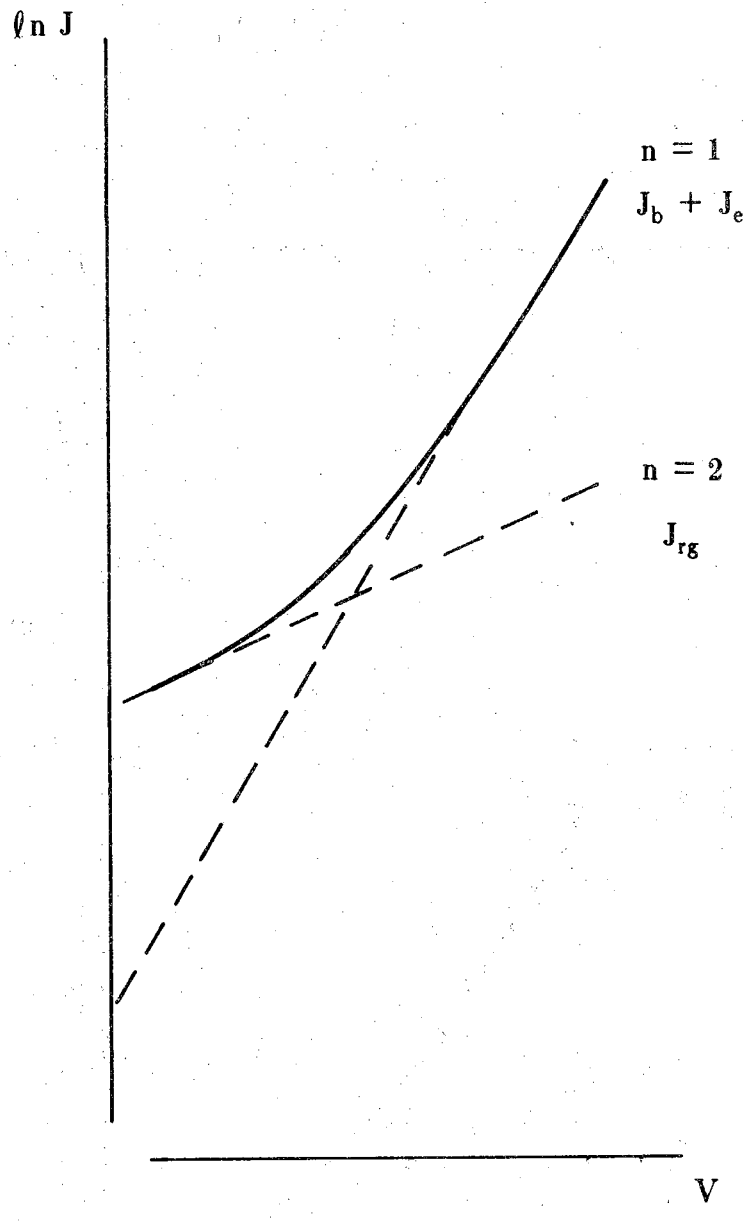

Figure 1.7 Dark J-V Characteristic.

1.3 Recombination Measurements in Solar Cells

Having presented the fundamentals of solar cell operation and the details of minority carrier recombination in the solar cell, we now attempt to infer from experimental measurement the amount of recombination in three solar cell types.

An important assumption made for all three of the cell types under study is that of base domination. By base domination, we mean that the dark current, J_{dark}, which normally consists of base, emitter, and space-charge components, is determined completely by the base component. That is, $J_{dark} = J_b$.

For the first two solar cell types which we will consider, the long base P^+N solar cell and the short base P^+N solar cell, we find the measurement of J_o to be sufficient in describing the cell recombination. However, for the third solar cell type, the short base P^+N solar cell with a back surface field (known as the P^+NN^+ BSF solar cell), we find this measurement to be inadequate in describing the recombination. For analyzing recombination in the BSF solar cell the measurements by the Rose-Weaver Method are more useful.

1.3.1 The Long Base P^+N Solar Cell

The simplest type of solar cell is the long base P^+N solar cell. The long base assumption implies that the base width is so much greater than the hole diffusion length, $W >> L_p$, that back surface recombination contributes negligibly to the total dark current. Under these circumstances, basic reference texts [5] give the base component of the total saturation current as

$$J_{bo} = \frac{q n_i^2}{N_D} \left(\frac{D_p}{\tau_p} \right)^{1/2} \tag{1.14}$$

where n_i is the intrinsic carrier concentration in the base and N_D is the base doping.

We now make the assumption that the solar cell is base dominated. Under base domination, minority carrier losses in the emitter and the space-charge region are neglected. Recombination occurs entirely in the base region. For base domination, $J_{dark} = J_b$, or, as follows from Equations 1.12 and 1.13, $J_o = J_{bo}$. Thus, by inferring J_o from J_{sc}–V_{oc} data and using published values for the intrinsic carrier concentration, n_i, the diffusion coefficient, D_p, and the base doping, N_D, we can solve for the minority carrier lifetime in the quasi-neutral base region from Equation 1.14. Rearranging,

$$\tau_p = \frac{D_p}{\left(\frac{J_o N_D}{q n_i^2}\right)^2} \quad (1.15)$$

Thus, we completely describe recombination in the long base P^+N solar cell by the minority hole lifetime, τ_p, in the quasi-neutral base.

1.3.2 The Short Base P^+N Solar Cell

For various reasons, such as reduced cost, higher radiation tolerance, and improved power-to-weight ratio [4], one might choose to design solar cells with base widths on the order of the minority carrier diffusion length in the base or shorter. When the diffusion length is comparable to the base width, the recombination of excess minority carriers occurs not only in the quasi-neutral base but at the back surface of the cell as well. To fully describe the recombination, we find it necessary then to consider both the minority carrier lifetime in the quasi-neutral base, τ_p, and the back surface recombination velocity for holes, S_{p_m}. The subscript m on S_p reminds us that the back surface of the cell is an ohmic contact.

At an ohmic contact, we recall, the surface recombination velocity is extremely large, approaching the thermal velocity limit. Since the recombination current at a surface must remain finite, it is evident from Equation 1.10 that the excess minority hole concentration at the contact must reduce to essentially zero. That is, $\Delta p_n = 0$. This boundary condition gives the base component of the total saturation current as [4]

$$J_{bo} = \frac{q n_i^2}{N_D}\left(\frac{D_p}{\tau_p}\right)^{1/2} \coth\left(\frac{W}{\sqrt{D_p \tau_p}}\right). \quad (1.16)$$

For a base dominated cell, we recall that $J_o = J_{bo}$. Therefore, by inferring J_o from J_{sc}–V_{oc} data and using published values for n_i, D_p, and N_D as before, we can solve for τ_p from

$$J_o \doteq \frac{q n_i^2}{N_D}\left(\frac{D_p}{\tau_p}\right)^{1/2} \coth\left(\frac{W}{\sqrt{D_p \tau_p}}\right). \quad (1.17)$$

Again, the minority carrier lifetime for holes in the quasi-neutral base, τ_p, completely describes the recombination in the short base P^+N solar cell.

1.3.3 The P^+NN^+ BSF Solar Cell

Significant improvement in short base solar cell performance can be achieved by the insertion a high-low junction just in front of the back ohmic contact (Figure 1.8). Such a cell is known as the back surface field, or BSF, solar cell. The equilibrium band diagram in Figure 1.9 illustrates the advantages of the BSF solar cell. From the diagram, we observe that the high-low junction creates a potential barrier to the minority carrier holes at the back of the solar cell. Holes that previously would have been lost to the high recombination of the back ohmic contact are now repelled from the back surface and more likely to diffuse back to the P-N junction to be collected. The BSF solar cell provides, in effect, a back surface of low surface recombination velocity in place of the ohmic contact with nearly infinite surface recombination velocity. Typical values of the surface recombination velocity due to the back surface field are reported in the literature between 10 and 10^4 cm–sec^{-1} [7].

The boundary condition at the back surface field is then

$$J_p\Big|_{\text{at BSF}} = qS_{p_{\text{eff}}}\Delta p_n\Big|_{\text{at BSF}} \tag{1.18}$$

where $S_{p_{\text{eff}}}$ is the effective back surface recombination velocity for holes. Importantly, $S_{p_{\text{eff}}}$ is finite and, therefore, Δp_n is not zero. In this instance, the base component of the total saturation current becomes [4]

$$J_{bo} = \frac{qn_i^2}{N_D}\left(\frac{D_p}{\tau_p}\right)^{1/2}\left[\frac{S_{p_{\text{eff}}}\left(\frac{\tau_p}{D_p}\right)^{1/2} + \tanh\left(\frac{W}{\sqrt{D_p\tau_p}}\right)}{1 + S_{p_{\text{eff}}}\left(\frac{\tau_p}{D_p}\right)^{1/2}\tanh\left(\frac{W}{\sqrt{D_p\tau_p}}\right)}\right]. \tag{1.19}$$

Since all later discussions will concern the BSF solar cell, we will now drop the special notation for $S_{p_{\text{eff}}}$ and just write S_p with the understanding that S_p is actually the effective back surface recombination velocity for holes at the back surface field of the solar cell.

Despite assuming the base dominated case and using published values for n_i, D_p, and N_D as before, we discover that we have only the measurement of the total saturation current, J_o, with which to find two unknowns: the minority carrier lifetime in the quasi-neutral base, τ_p, and the effective back surface recombination velocity for holes, S_p. Clearly, to properly analyze recombination

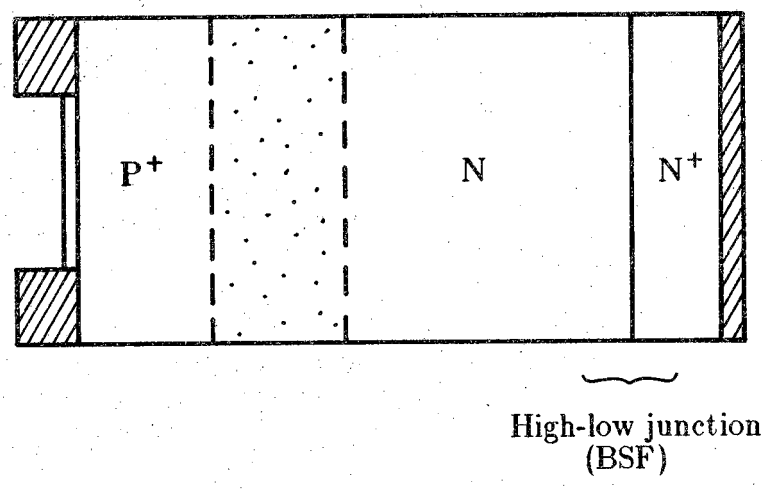

Figure 1.8 P^+NN^+ BSF Solar Cell.

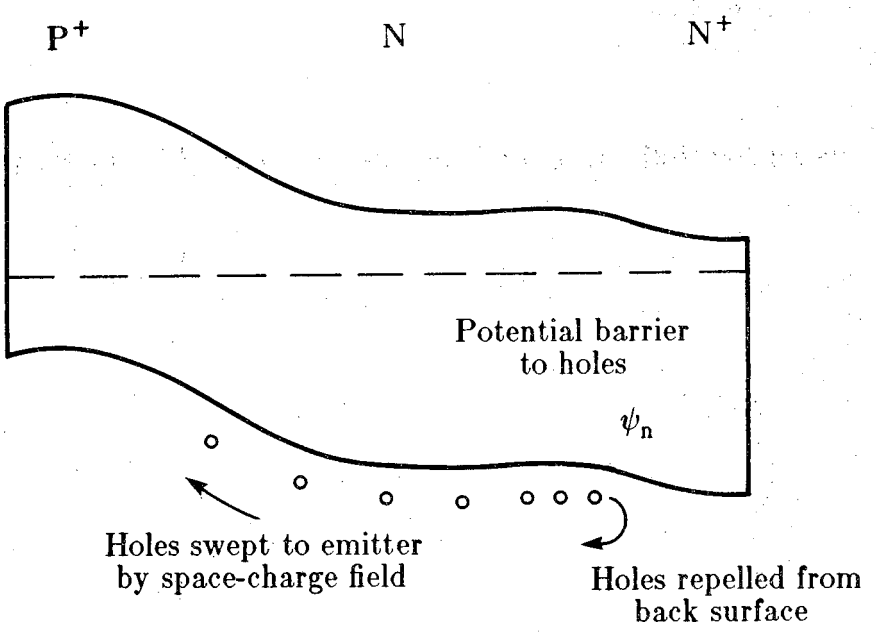

Figure 1.9 Equilibrium Band Diagram of the BSF Solar Cell.

in high efficiency BSF solar cells, we need to develop an experimental technique permitting a greater number of measurements.

Chapter II discusses the merits of one such measurement technique, known as the Rose-Weaver Method. Of special interest in this chapter is the development of the Rose-Weaver Model to relate the measurements to the underlying physical theory. Chapter III then discusses the important contribution of S. C. Jain, which results in an improved version of the Rose-Weaver Model. Finally, Chapter IV describes a simultaneous solution method for the model enabling one to find values for the desired recombination quantities independently of empirical data for n_i, D_p, and N_D. This thesis concludes by discussing the significance of the results and offering recommendations for further analysis of the recombination.

CHAPTER II
THE ROSE-WEAVER METHOD

The Rose-Weaver Method [3], as indicated in Chapter I, is an experimental technique permitting the determination of recombination in BSF solar cells. Specifically, the Rose-Weaver Method permits the determination of τ_p, the minority carrier hole lifetime in the quasi-neutral base, and S_p, the effective back surface recombination velocity for holes, in a BSF solar cell through measurement of the short circuit current and the open circuit voltage decay rates. These measurements may be described rather simply. We use a light source to establish steady-state short circuit current and open circuit voltage conditions in the solar cell. We then remove the light source and allow the solar cell to relax to the equilibrium state in the dark. The rates of these two decays constitute the Rose-Weaver measurements. Later, we shall see that the actual measurement of the decay rates is somewhat different than described above.

Essential to the Rose-Weaver Method is the development of a model to relate the experimental measurement of the short circuit current and open circuit voltage decay rates to the underlying physics. The model forms a system of four equations. Given the decay rate measurements, we then solve these four equations simultaneously to determine τ_p and S_p. Two other unknowns, β_J and β_V, are also found but serve only an ancillary role in the solution of the system.

The purpose of this chapter is to discuss the derivation of the Rose-Weaver Model. The derivation begins in the first section of this chapter with the identification of the problem. The problem is to find the minority carrier concentration in the base as a function of space and time during the short circuit current and open circuit voltage decay. Our efforts focus therefore on investigating the continuity equation for minority carriers in the base. In the second section, we construct solutions to the continuity equation. These solutions form the basis of the Rose-Weaver Model. In the third section, we describe how these solutions for the minority carrier concentration can be related to the measurements of the short circuit current and open circuit

voltage decay. In the fourth section, we present the Rose-Weaver Model in its final form as a system of equations which, when given the decay rate measurements, can be solved simultaneously for τ_p and S_p. We conclude the chapter with a discussion of the experimental apparatus used by Rose and Weaver to measure the short circuit current and the open circuit voltage decay rates.

2.1 Problem Definition

The problem to be analyzed in the derivation of the Rose-Weaver Model is, as stated in the introduction, to find the space and time dependence of the minority carrier concentration in the base during the short circuit current and open circuit voltage decay. We define the problem mathematically by considering the base geometry, by writing the continuity equation for the minority carrier concentration in the base, and by specifying the conditions for the minority carrier concentration at the boundaries of the base.

2.1.1 Base Geometry

Having assumed to this point a solar cell dominated by base recombination, we restrict our analysis to just the quasi-neutral base region and its boundaries as shown in Figure 2.1. The left boundary, $x = 0$, defines the space-charge edge of the quasi-neutral base. For varying junction biases, such as those found under the short circuit current and open circuit voltage conditions, the space-charge edge of the quasi-neutral base actually moves. The amount of movement is small (less than a micron) and is negligible compared to the width of the base which is typically several hundred microns. The right boundary, $x = W$, indicates the effective back surface for the minority carriers in the quasi-neutral base. This boundary is fixed with respect to the junction bias.

Note that for consistency with Chapter I we have chosen to study the P^+NN^+ BSF solar cell. Hence, the base region is n-type and the minority carriers in the base are holes.

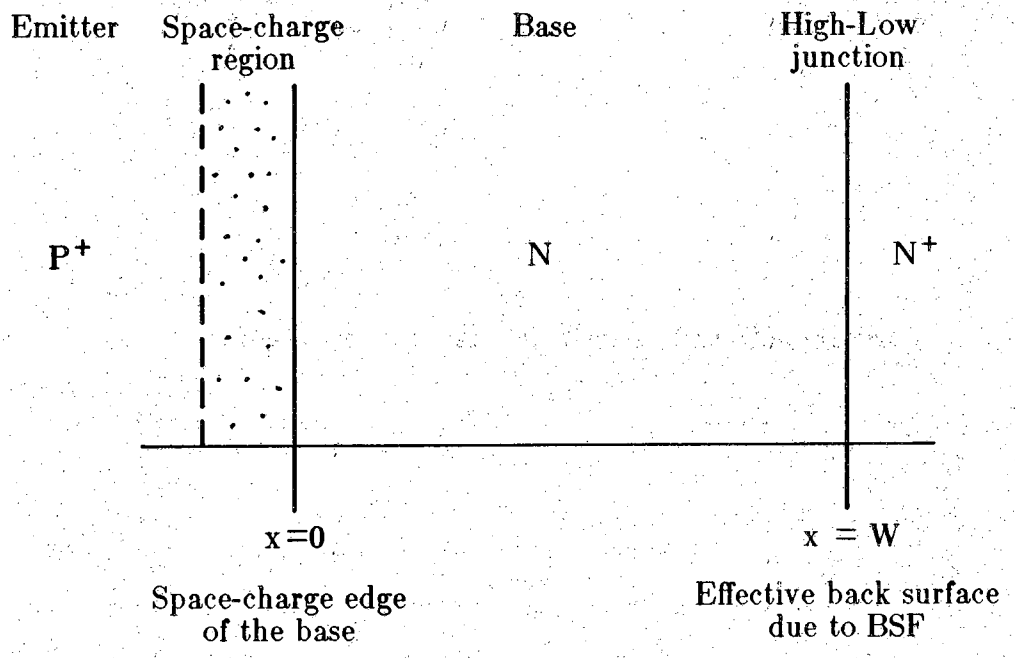

Figure 2.1 Solar Cell Base and its Boundaries.

2.1.2 Continuity Equation

The continuity equation for minority carrier holes in the quasi-neutral base is

$$D_p \frac{\partial^2 \Delta p_n}{\partial x^2} - \frac{\Delta p_n}{\tau_p} = \frac{\partial \Delta p_n}{\partial t} \tag{2.1}$$

where Δp_n, the excess hole concentration, is defined as

$$\Delta p_n = p_n - p_{no}. \tag{2.2}$$

p_n is the total hole concentration, while p_{no} is the equilibrium hole concentration and is given by

$$p_{no} = \frac{n_i^2}{N_D}. \tag{2.3}$$

In writing the above equation, we have made the following assumptions:

[1] the excess hole concentration in the quasi-neutral base, Δp_n is a function of space, x, and time, t.

[2] low level injection conditions exist for the excess hole concentration in the quasi-neutral base.

[3] no carrier generation exists in the quasi-neutral base once the photon excitation has been removed.

[4] no electric fields are present in the quasi-neutral base.

[5] the doping, N_D, and the intrinsic carrier concentration, n_i, are constant throughout the quasi-neutral base. Hence, the equilibrium hole concentration, p_{no}, is constant throughout the quasi-neutral base as seen from Equation 2.3.

[6] the diffusion coefficient for holes, D_p, is constant throughout the quasi-neutral base.

[7] since the emitter width and space-charge region width are small compared to the quasi-neutral base width, we treat the quasi-neutral base width and the total device width as interchangeable.

2.1.3 Boundary Conditions

We are interested in two specific cases of the solar cell operation: the short circuit current case and the open circuit voltage case. Thus, we must formulate two sets of boundary conditions for the minority carrier holes in the quasi-neutral base.

2.1.3.1 Short Circuit Current Case

At $x = 0$, we apply the law of the junction [5]

$$\Delta p_n = p_{n_o}\left[\exp\left(\frac{V}{V_T}\right) - 1\right]. \tag{2.4}$$

Under the short circuit current condition, the applied voltage across the junction, V, equals zero. Hence, our first boundary condition is

$$\Delta p_n\Big|_{x=0} = 0. \tag{2.5}$$

At $x = W$, we define the minority carrier hole current lost to recombination at the BSF in terms of the effective back surface recombination velocity, S_p. Adapting Equation 1.18, we write

$$J_p\Big|_{x=W} = qS_p\,\Delta p_n\Big|_{x=W}. \tag{2.6}$$

The current density in the above expression is related to the gradient of the excess minority carrier hole concentration [5] by

$$J_p\Big|_{x=W} = -qD_p\,\frac{\partial \Delta p_n}{\partial x}\Big|_{x=W}. \tag{2.7}$$

Combining the two equations above, we obtain our second boundary condition,

$$\frac{\partial \Delta p_n}{\partial x}\Big|_{x=W} = -\frac{S_p}{D_p}\,\Delta p_n\Big|_{x=W}. \tag{2.8}$$

2.1.3.2 Open Circuit Voltage Case

At x = 0, we assume that the total current can be attributed entirely to the flow of minority carriers. Moreover, we assume that the base component of this current is dominant over the emitter and space-charge components. In other words, we neglect the recombination at the front surface, in the quasi-neutral emitter, and in the space-charge region, while considering only the recombination in the quasi-neutral base and at the effective back surface. (In Chapter III, we will remove the assumption of base domination and allow for emitter recombination by invoking the Jain analysis). Remembering that the total current through the solar cell under the open circuit condition is zero and applying the above assumptions, we conclude that

$$J_{oc} = J_p\Big|_{x=0} = -qD_p \left.\frac{\partial \Delta p_n}{\partial x}\right|_{x=0} = 0. \tag{2.9}$$

After simplification, the first boundary condition for the open circuit voltage case is just

$$\left.\frac{\partial \Delta p_n}{\partial x}\right|_{x=0} = 0. \tag{2.10}$$

The boundary condition at x = W remains the same as in the short circuit current case and is repeated here for completeness

$$\left.\frac{\partial \Delta p_n}{\partial x}\right|_{x=W} = -\frac{S_p}{D_p}\Delta p_n\Big|_{x=W}. \tag{2.11}$$

2.2 Solution of the Continuity Equation

The separation of variables technique provides a general solution to the continuity equation for the minority carrier hole concentration in the base. In the preceding section, the consideration of the short circuit current and the open circuit voltage conditions has led to two sets of boundary conditions for the minority carrier hole concentration in the base. The application of the boundary conditions to the continuity equation results therefore in two particular solutions--one for the short circuit current case and the other for the open circuit voltage case.

2.2.1 Separation of Variables

The general solution to the continuity equation is found by the separation of variables technique [8]. To indicate the dependence of Δp_n on space and time, we write the continuity equation as

$$D_p \frac{\partial^2 \Delta p_n(x,t)}{\partial x^2} - \frac{\Delta p_n(x,t)}{\tau_p} = \frac{\partial \Delta p_n(x,t)}{\partial t} . \tag{2.12}$$

Then separating variables by setting $\Delta p_n(x,t) = P(x)T(t)$ and equating the result to a separation constant, β, we find

$$\frac{P''(x)}{P(x)} = \frac{1}{D_p}\left[\frac{T'(t)}{T(t)} + \frac{1}{\tau_p}\right] = -\beta^2. \tag{2.13}$$

The solution of the space part is

$$P(x) = C_1 \cos \beta x + C_2 \sin \beta x, \tag{2.14}$$

while the solution of the time part is

$$T(t) = \exp\left[-\left(\beta^2 D_p + \frac{1}{\tau_p}\right)t\right]. \tag{2.15}$$

The general solution is, therefore,

$$\begin{aligned} \Delta p_n(x,t) &= P(x)T(t) \\ &= \left(C_1 \cos \beta x + C_2 \sin \beta x\right) \cdot \exp\left[-\left(\beta^2 D_p + \frac{1}{\tau_p}\right)t\right]. \end{aligned} \tag{2.16}$$

2.2.2 Application of the Boundary Conditions

We now find the particular solutions to the continuity equation by applying the boundary conditions for the short circuit current and the open circuit voltage cases.

2.2.2.1 Short Circuit Current Case

Applying the short circuit current boundary conditions from Section 2.1.3.1 to the general solution, Equation 2.16, we find

$$\Delta p_{n_J}(x,t) = C_J \sin \beta_J x \cdot \exp\left[-\left(\beta_J^2 D_p + \frac{1}{\tau_p}\right)t\right] \tag{2.17}$$

where

$$\beta_J \cot \beta_J W = -\frac{S_p}{D_p} \tag{2.18}$$

and C_J is an arbitrary constant. The subscript J refers to the short circuit current condition.

To satisfy the initial conditions, we write the solution as an infinite series such that

$$\Delta p_{n_J}(x,t) = \sum_{m=1}^{\infty} C_{J_m} \sin \beta_{J_m} x \cdot \exp\left[-\left(\beta_{J_m}^2 D_p + \frac{1}{\tau_p}\right)t\right] \tag{2.19}$$

where

$$\beta_{J_m} \cot \beta_{J_m} W = -\frac{S_p}{D_p}. \tag{2.20}$$

The solution we have derived above provides us with two useful results. The first result is an expression, Equation 2.20, for the short circuit current decay eigenvalue, β_{J_m}. The second result is found by inspecting the time part of Equation 2.19. From the time part, we find an expression for the decay rate of the excess minority carrier hole concentration under short circuit current conditions. This expression is

$$\frac{1}{\tau_{J_m}} = \beta_{J_m}^2 D_p + \frac{1}{\tau_p} \tag{2.21}$$

where τ_{J_m} is the short circuit current decay rate of mode m.

2.2.2.2 Open Circuit Voltage Case

For the open circuit voltage case, our analysis proceeds in a fashion similar to the short circuit current case. Applying the open circuit voltage boundary conditions found in Section 2.1.3.2 to the general solution, Equation 2.16, we find

$$\Delta p_{n_V}(x,t) = C_V \cos \beta_V x \cdot \exp\left[-\left(\beta_V^2 D_p + \frac{1}{\tau_p}\right)t\right] \tag{2.22}$$

where

$$\beta_V \tan \beta_V W = \frac{S_p}{D_p} \tag{2.23}$$

and C_V is an arbitrary constant. The subscript V refers to the open circuit voltage condition.

Again, to satisfy the initial conditions, we write the solution as an infinite series such that

$$\Delta p_{n_V}(x,t) = \sum_{m=1}^{\infty} C_{V_m} \cos \beta_{V_m} x \cdot \exp\left[-\left(\beta_{V_m}^2 D_p + \frac{1}{\tau_p}\right)t\right] \tag{2.24}$$

where

$$\beta_{V_m} \tan \beta_{V_m} W = \frac{S_p}{D_p} . \tag{2.25}$$

As in the short circuit current case, we find two useful results from the solution derived above. The first result is an expression, Equation 2.25, for the open circuit voltage decay eigenvalue, β_{v_m}. The second result is found by inspecting the time part of Equation 2.24. From the time part, we find an expression for the decay rate of the excess minority carrier hole concentration under open circuit voltage conditions. This expression is

$$\frac{1}{\tau_{V_m}} = \beta_{V_m}^2 D_p + \frac{1}{\tau_p} \tag{2.26}$$

where τ_{V_m} is the open circuit voltage decay rate of mode m.

2.3 Measurement of the Decay Rates

In the preceding section, our analysis of the short circuit current and open circuit voltage decay has given us four useful results. These results are just the two eigenvalue expressions (Equations 2.20 and 2.25) and the two expressions for the decay rates of the excess minority hole concentration (Equations 2.21 and 2.26). The decay rates of the excess minority hole concentration, unfortunately, are internal variables which cannot be measured directly. However, we can measure the rates of the short circuit current and open circuit

voltage decay. It is now necessary to relate the decay rates of the excess minority carrier hole concentration to the measurable rates of the short circuit current and open circuit voltage decay.

2.3.1 Short Circuit Current Decay Rate

The short circuit current can be written in terms of the excess minority carrier concentration as follows

$$J_{sc}(t) = qD_p \left.\frac{\partial \Delta p_{n_J}(x,t)}{\partial x}\right|_{x=0} \tag{2.27}$$

where $\Delta p_{n_J}(x,t)$ is the excess minority carrier hole concentration under short circuit conditions given in Equation 2.19. An equivalent term for the emitter component of the short circuit current is assumed to be negligible in comparison with the base component and therefore is not included in the above equation. Evaluating the expression above then, we obtain the result

$$J_{sc}(t) = \sum_{m=1}^{\infty} J_{sc_m} \exp\left[-\frac{t}{\tau_{J_m}}\right] \tag{2.28}$$

where

$$\frac{1}{\tau_{J_m}} = \beta_{J_m}^2 D_p + \frac{1}{\tau_p} \tag{2.29}$$

and

$$J_{sc_m} = qD_p C_{J_m} \beta_{J_m}. \tag{2.30}$$

A study of the allowed eigenvalues for β_{J_m} indicates that the decay rates of the individual modes progressively decrease as m increases (see Appendix A). Actual plots of the short circuit current decay, in fact, demonstrate that after a sufficient wait the higher order terms decay to insignificant levels, leaving just the first order dependence [3]. Thus,

$$J_{sc}(t) = J_{sc_1} \exp\left[-\frac{t}{\tau_{J_1}}\right]. \tag{2.31}$$

The short circuit current decay rate is therefore described in the asymptotic region (where higher order decay terms are negligible) by τ_{J_1} where

$$\frac{1}{\tau_{J_1}} = \beta_{J_1}^2 D_p + \frac{1}{\tau_p} . \tag{2.32}$$

The measurement of this decay rate is obtained from a plot of the logarithm of the short circuit current versus time as shown in Figure 2.2. The decay rate is just the negative reciprocal of the slope in the asymptotic region of the plot.

2.3.2 Open Circuit Voltage Decay Rate

The open circuit voltage can be written in terms of the excess minority carrier concentration through the law of the junction (Equation 2.4). Thus,

$$V_{oc}(t) = n V_T \ln\left[\frac{\Delta p_{n_V}(x,t)}{p_{no}} + 1\right]\Bigg|_{x=0} \tag{2.33}$$

where $\Delta p_{n_V}(x,t)$ is the excess minority carrier hole concentration under open circuit conditions given in Equation 2.24. Also in the equation are the thermal voltage, V_T, the junction quality factor, n, and the equilibrium minority carrier hole concentration, p_{no}.

There are problems, however, with the above description of the open circuit voltage decay. The problems arise because the law of the junction, in its present form, does not correctly describe the open circuit voltage as it decays from the steady-state illumination value (0.6 volts, for example) to its equilibrium value in the dark (0 volts). As the junction voltage steadily decreases during the decay, the effects of space-charge recombination become increasingly important. Indeed, the junction quality factor in Equation 2.33, rather than being constant, is a continuous function of open circuit voltage. Thus, large signal measurements of the open circuit voltage decay are not particularly useful, unless we wish to constantly monitor the value of n during the decay rate measurements. Furthermore, at low voltage levels, the decay of the open circuit voltage is dominated by the junction RC time constant [9].

To avoid the difficulties encountered at the lower voltage levels during the open circuit voltage decay, Rose and Weaver apply a light bias to ensure solar cell operation far above the voltages at which the space-charge recombination and the junction RC time constant are significant [3]. The measurement of the open circuit voltage decay rate is then made by studying the response of the open circuit voltage to a small photon excitation about the light bias [9]. We can still use the law of the junction, however we must now modify the minority carrier concentration to include dc and small signal components.

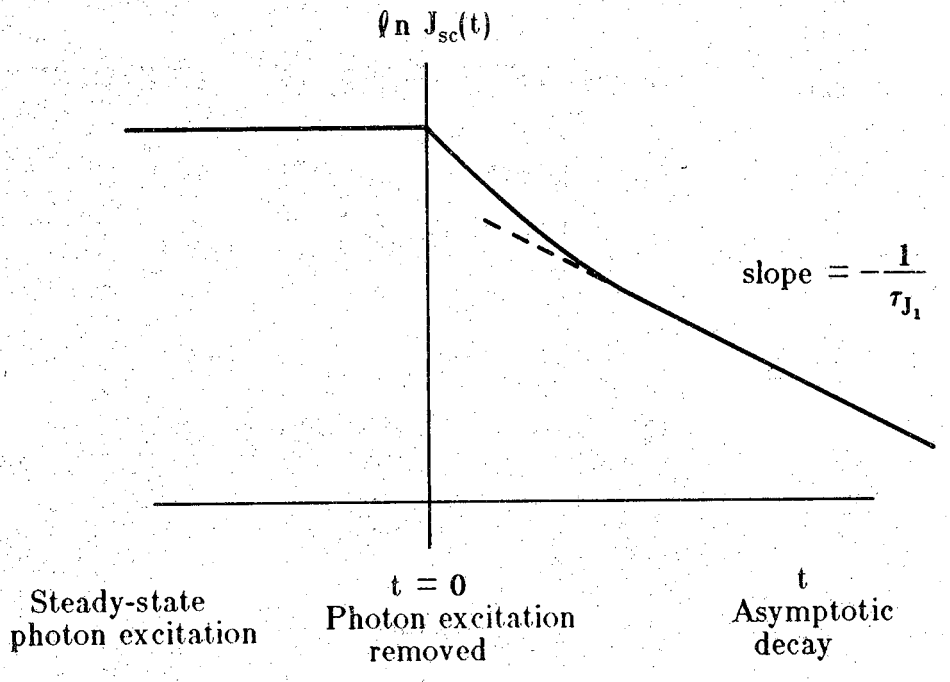

Figure 2.2 Measurement of the Short Circuit Current Decay Rate.

Accordingly, Equation 2.33 becomes

$$V_{oc}(t) = n V_T \ln\left[\frac{\Delta p_{n_B} + \Delta p_{n_V}(x,t)}{p_{no}} + 1\right]\Bigg|_{x=0} \tag{2.34}$$

where Δp_{n_B} refers to the excess minority carrier hole concentration created by the light bias and $\Delta p_{n_V}(x,t)$ represents the excess minority carrier hole concentration responding to the small photon excitation about the light bias.

Assuming $\left[\Delta p_{n_B} + \Delta p_{n_V}(x,t)\right]/p_{no} >> 1$ and making the small signal approximation $\Delta p_{n_V}(x,t) << \Delta p_{n_B}$ (see Appendix B), we find

$$V_{oc}(t) = V_B + \sum_{m=1}^{\infty} V_{oc_m} \exp\left[-\frac{t}{\tau_{V_m}}\right] \tag{2.35}$$

where

$$V_B = n V_T \ln\left[\frac{\Delta p_{n_B}}{p_{no}}\right], \tag{2.36}$$

$$V_{oc_m} = \frac{n V_T}{\Delta p_{n_B}} C_{V_m}, \tag{2.37}$$

and

$$\frac{1}{\tau_{V_m}} = \beta_{V_m}^2 D_p + \frac{1}{\tau_p}. \tag{2.38}$$

An analysis similar to that presented for the short circuit current case indicates that the open circuit voltage decay rates of the individual modes progressively decrease as m increases. Moreover, actual plots of the open circuit voltage decay demonstrate, as before, the importance of just the first order decay term after a sufficient time delay. Thus, Equation 2.35 becomes

$$V_{oc}(t) = V_B + V_{oc_1} \exp\left[-\frac{t}{\tau_{V_1}}\right]. \tag{2.39}$$

The open circuit voltage decay rate is therefore described in the asymptotic region (where higher order decay terms are negligible) by τ_{V_1} where

$$\frac{1}{\tau_{V_1}} = \beta_{V_1}^2 D_p + \frac{1}{\tau_p}. \tag{2.40}$$

The measurement of this decay rate is obtained from a plot of the logarithm of the open circuit voltage versus time as shown in Figure 2.3. The decay rate is

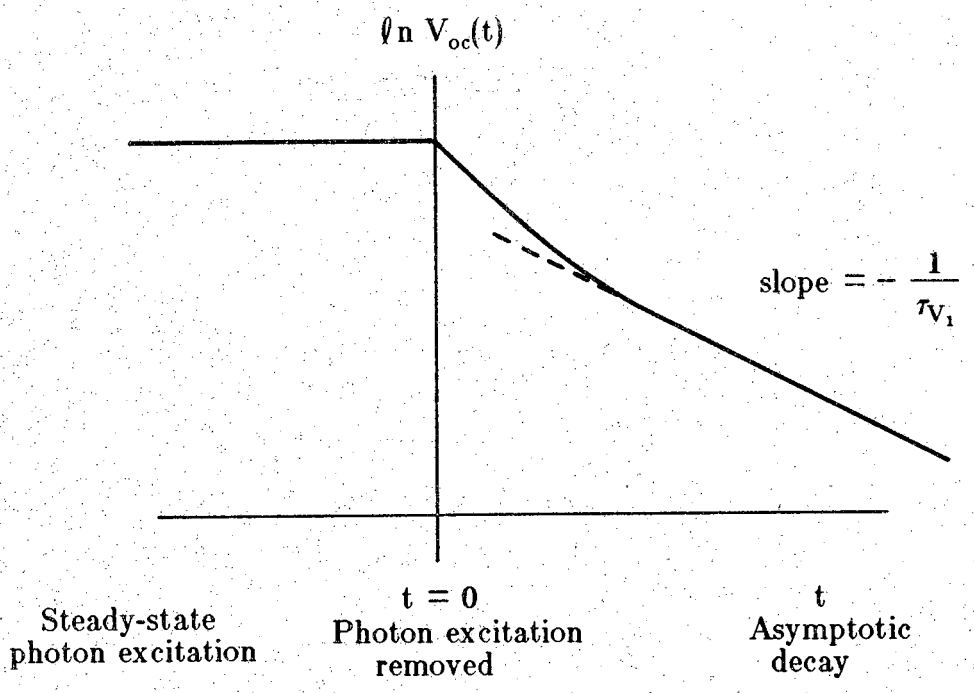

Figure 2.3 Measurement of the Open Circuit Voltage Decay Rate.

just the negative reciprocal of the slope in the asymptotic region of the plot. Furthermore, note that the decay rate is independent of the junction quality factor.

2.4 Rose-Weaver Model Equations

The results of the Rose-Weaver analysis form a system of four simultaneous equations which we present below:

$$\beta_J \cot \beta_J W = -\frac{S_p}{D_p} \tag{2.41}$$

$$\beta_V \tan \beta_V W = \frac{S_p}{D_p} \tag{2.42}$$

$$\frac{1}{\tau_J} = \beta_J^2 D_p + \frac{1}{\tau_p} \tag{2.43}$$

$$\frac{1}{\tau_V} = \beta_V^2 D_p + \frac{1}{\tau_p} . \tag{2.44}$$

This system of equations is appropriately called the Rose-Weaver Model. We have dropped the subscript m = 1 in the equations above with the understanding that only the first term of the infinite series solution is significant in the asymptotic region of the transient decay.

Measuring τ_J, τ_V, and W, and determining D_p from base resistivity data, we can now solve for the minority carrier hole lifetime in the quasi-neutral base, τ_p, and the effective back surface recombination velocity for holes, S_p, in the BSF solar cell. Note that the eigenvalues β_J and β_V are interesting only as auxiliary variables to the solution.

2.5 Rose-Weaver Experimental Apparatus

We now briefly describe the experimental apparatus used by Rose and Weaver to measure the short circuit current and open circuit voltage decay [3]. In Figure 2.4, we observe the solar cell in a simple test circuit. The circuit can be opened or closed with the circuit switch to provide the proper conditions for the measurement of the short circuit current and open circuit voltage decay. A NdYAG laser is used to supply photons to the solar cell through an optical switch. Initially, the optical switch is open and the solar cell permitted to

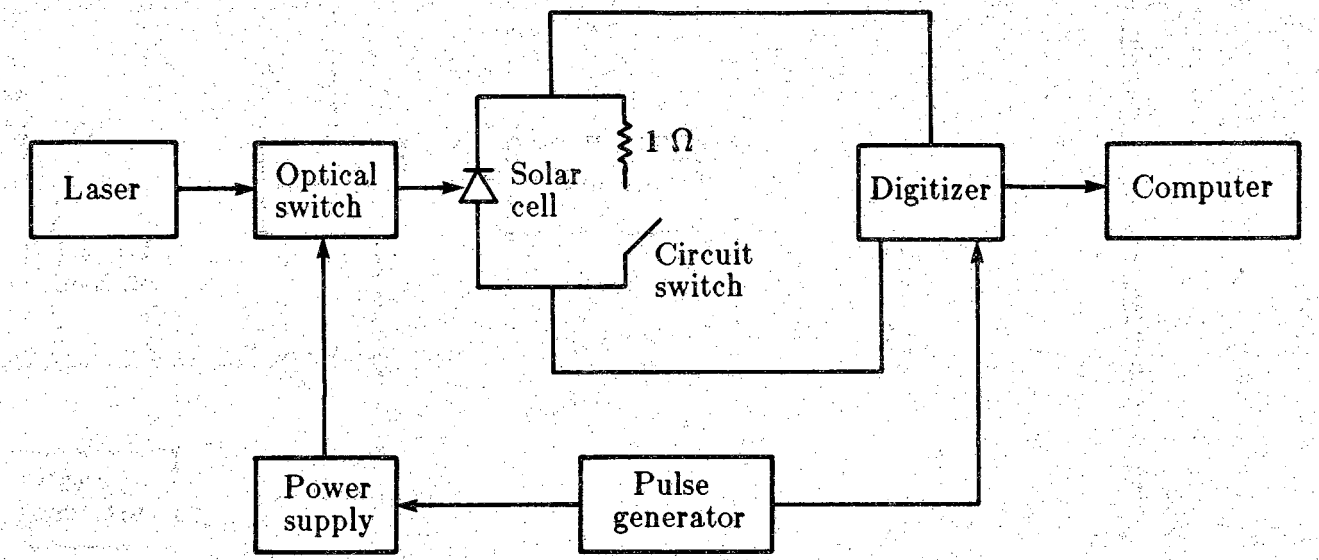

Figure 2.4 Rose-Weaver Experimental Apparatus.

reach a steady state condition of either the short circuit current or open circuit voltage. A pulse generator then closes the optical switch. At the same time, the pulse from the generator triggers the digitizer to begin taking the transient decay information from the solar cell. An HP computer then records the data and calculates the rate of transient decay.

CHAPTER III
THE ROSE-WEAVER-JAIN MODEL

In the derivation of the Rose-Weaver Model a major assumption is made. It is assumed, in order to simplify the analysis, that minority carrier recombination occurs only in the quasi-neutral base and at the effective back surface of the BSF solar cell. Neglected are the contributions to the dark current which arise from recombination at the front surface, in the quasi-neutral emitter, and in the space-charge region of the solar cell. Thus, the Rose-Weaver analysis, using the terminology introduced in Chapter I, assumes that the base component of the total recombination dominates over the emitter and space-charge region components.

While Rose and Weaver have devised measurement techniques which make negligible the effect of space-charge recombination, experiments with surface passivation [10] and sample calculations using typical Auger lifetimes and Slotboom bandgap narrowing data [11] indicate that emitter recombination can form a significant portion of the total solar cell recombination. Quite clearly, it is necessary to restructure the Rose-Weaver analysis in order that the effect of emitter recombination be included. To accomplish such a task requires that we re-evaluate each part of the Rose-Weaver analysis (the continuity equation, the boundary conditions for the minority carrier concentration under short circuit current and open circuit voltage conditions, and the expressions for the decay rates of the short circuit current and open circuit voltage) in terms of emitter recombination.

The initial consequence of considering emitter recombination in the Rose-Weaver analysis is a revised boundary condition for the minority carriers at the space-charge edge of the base under open circuit voltage conditions. This corrected boundary condition, presented by S. C. Jain [12], expresses the coupling which in general exists between the base and emitter recombination. Completing the Rose-Weaver analysis with Jain's boundary condition leads, as expected, to a new set of Rose-Weaver Model equations. The key feature of the new set of equations is the introduction of the emitter component of the total saturation current, J_{eo}. In J_{eo} are lumped the effects of the front surface and

quasi-neutral emitter recombination. The Rose-Weaver Model, when emitter recombination is included, is termed the Rose-Weaver-Jain Model.

In the following pages, we systematically investigate the effect of emitter recombination in the Rose-Weaver analysis. In particular, we show the derivation of Jain's open circuit voltage boundary condition and how this boundary condition is applied to obtain the set of Rose-Weaver-Jain Model equations. Finally, we indicate how an experiment which removes the back surface field of the cell extends the usefulness of the Rose-Weaver-Jain Model by eliminating the model dependency on n_i, D_p, and N_D. As an aside, we verify throughout the discussion that the effects of space-charge recombination can indeed be neglected altogether.

3.1 The Effect of Emitter Recombination

The Rose-Weaver Method is an analysis of recombination in the solar cell base. To include the effects of emitter recombination we do not abandon completely the base analysis presented by Rose and Weaver. Rather, we again solve the continuity equation for the minority carrier concentration in the base. To allow for emitter effects we need only to rewrite the boundary conditions for the minority carrier concentration in the short circuit current and open circuit voltage cases, and to redefine the decay rates of the short circuit current and open circuit voltage. We shall demonstrate that the effect of emitter recombination on the Rose-Weaver Model is provided entirely by the revised open circuit voltage boundary condition proposed by Jain.

3.1.1 Boundary Conditions

We investigate in this section the effect of emitter recombination on the boundary conditions for the minority carrier concentration in the base under the short circuit current and open circuit voltage cases.

3.1.1.1 Short Circuit Current Case

The law of the junction at the space-charge edge of the base,

$$\Delta p_n = p_{no}\left[\exp\left(\frac{V}{V_T}\right) - 1\right], \tag{3.1}$$

remains valid regardless of emitter recombination. Hence, our short circuit current boundary condition at x = 0 is still

$$\Delta p_n(x,t)\Big|_{x=0} = 0. \tag{3.2}$$

Note that this boundary condition actually decouples the base recombination from the emitter recombination, permitting the analysis to proceed solely in the base. We observe, as well, that for zero voltage across the junction the Shockley-Hall-Read theory predicts zero space-charge recombination [5]. Thus, the contention that space-charge recombination can be neglected in the Rose-Weaver analysis has been justified for short circuit current conditions.

The recombination at the effective back surface of the solar cell is described completely in terms of the excess minority carrier hole concentration in the base and is, therefore, independent of emitter and space-charge effects. Thus, the boundary condition at x = W for the short circuit current case is unchanged from that in the Rose-Weaver analysis,

$$\frac{\partial \Delta p_n(x,t)}{\partial x}\bigg|_{x=W} = -\frac{S_p}{D_p}\Delta p_n(x,t)\bigg|_{x=W}. \tag{3.3}$$

In summary, emitter recombination and space-charge recombination have no effect on the solution for the minority carrier concentration in the base under short circuit current conditions. Hence, the solution derived in Chapter II for the case of base domination is still valid. The solution, repeated here for convenience, is

$$\Delta p_{n_J}(x,t) = \sum_{m=1}^{\infty} C_{J_m} \sin \beta_{J_m} x \cdot \exp\left[-\left(\beta_{J_m}^2 D_p + \frac{1}{\tau_p}\right)t\right] \tag{3.4}$$

where

$$\beta_{J_m} \cot \beta_{J_m} W = -\frac{S_p}{D_p} \tag{3.5}$$

and

$$\frac{1}{\tau_{J_m}} = \beta_{J_m}^2 D_p + \frac{1}{\tau_p}. \tag{3.6}$$

3.1.1.2 Open Circuit Voltage Case

We begin this section by reviewing our result from Chapter II. At x = 0, we assumed that the total current can be attributed entirely to the flow of minority carriers. Furthermore, we assumed that the base component of this current is dominant over the emitter and space-charge components. Using this assumption and noting that the total current through the solar cell under the open circuit voltage condition is zero, we derived the boundary condition

$$J_{oc} = J_p\Big|_{x=0} = -qD_p \left.\frac{\partial \Delta p_n(x,t)}{\partial x}\right|_{x=0} = 0. \tag{3.7}$$

Or, after simplification,

$$\left.\frac{\partial \Delta p_n(x,t)}{\partial x}\right|_{x=0} = 0. \tag{3.8}$$

To include the effect of emitter recombination, we follow the analysis of S. C. Jain [12]. The effect of space-charge recombination, we recall, is avoided by using the light-bias technique of Rose and Weaver discussed in Chapter II.

We begin the Jain analysis by rewriting the total current through the solar cell under the open circuit voltage condition as the sum of base and emitter components. Thus, at the junction,

$$J_{oc} = J_p\Big|_{x=0} + J_n\Big|_{x=0} = 0. \tag{3.9}$$

In terms of the base and emitter minority carrier concentrations, we have

$$-qD_p \left.\frac{\partial \Delta p_n(x_B,t)}{\partial x_B}\right|_{x_B=0}$$

$$+ qD_n \left[\frac{\partial \Delta n_p(x_E,t)}{\partial x_E} - \frac{q}{kT} E_E(x_E)\,\Delta n_p(x_E,t)\right]_{x_E=0} = 0 \tag{3.10}$$

where Δp_n is the excess minority hole concentration at the distance x_B into the base and at the time t, Δn_p is the excess minority electron concentration at the distance x_E into the emitter and at the time t, $E_E(x_E)$ is the electric field in the emitter arising from the impurity gradient and the variance of the bandgap narrowing with distance, and D_p and D_n are the hole and electron diffusion coefficients in the base and the emitter, respectively. Figure 3.1 illustrates the coordinate system used for the solar cell in the Jain analysis.

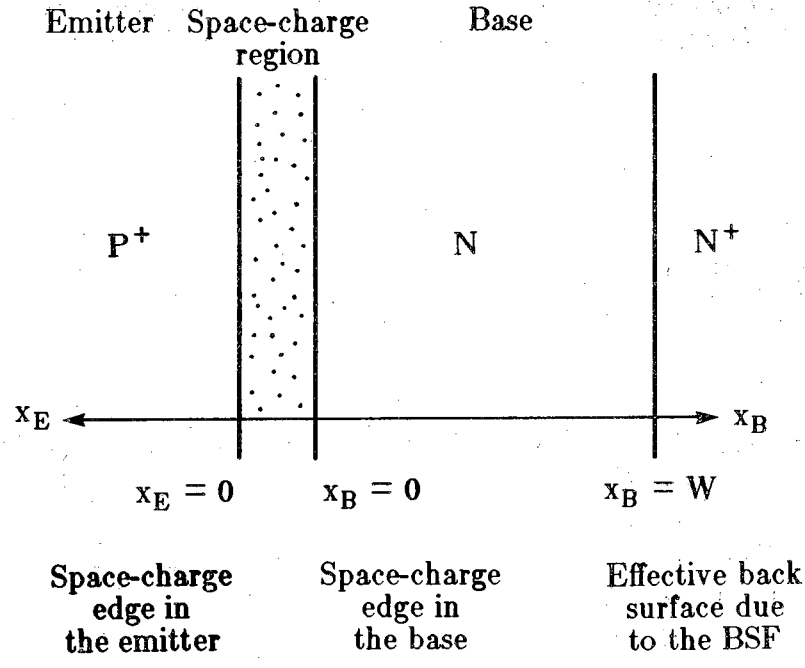

Figure 3.1 Solar Cell Coordinate System for the Jain Analysis.

The success of Jain's analysis relies on making the quasi-static emitter approximation [12]. In essence, Jain assumes that the minority carriers in the emitter decay so rapidly compared to the rate of open circuit voltage decay that the minority carriers in the emitter almost instantly reach the steady-state dark distribution. To support this assumption, we contend that decay rates, in general, correspond approximately in order of magnitude to minority carrier lifetimes. Therefore, we expect the decay rate in the emitter to be roughly on the order of nanoseconds. Since this decay rate is much faster than the decay rate measured for the open circuit voltage (typically on the order of microseconds), the quasi-static emitter approximation appears well founded.

Under the quasi-static emitter approximation, the second term in Equation 3.10 is interpreted as just the steady-state dark forward current of the solar cell emitter. Designating this steady-state dark forward current as J_{EF}, we recast Equation 3.10 in the following form

$$-qD_p \left.\frac{\partial \Delta p_n(x_B,t)}{\partial x_B}\right|_{x_B=0} + J_{EF} = 0. \tag{3.11}$$

The steady-state dark forward current in the emitter is related to the junction voltage through

$$J_{EF} = J_{eo}\left[\exp\left(\frac{V(t)}{nV_T}\right) - 1\right] \tag{3.12}$$

where J_{eo} is the emitter component of reverse saturation current and V(t) represents the open circuit junction voltage which decays with time. When the above relation is substituted into Equation 3.11, the result, upon rearrangement, is

$$qD_p \left.\frac{\partial \Delta p_n(x_B,t)}{\partial x_B}\right|_{x_B=0} = J_{eo}\left[\exp\left(\frac{V(t)}{nV_T}\right) - 1\right]. \tag{3.13}$$

However, the law of the junction, written at the base edge of the space-charge region, gives

$$\Delta p_n(x_B,t)\Big|_{x_B=0} = p_{no}\left[\exp\left(\frac{V(t)}{nV_T}\right) - 1\right]. \tag{3.14}$$

Substituting the above expression into Equation 3.13 and rearranging, we obtain Jain's boundary condition for the open circuit voltage condition at the base edge of the space-charge region. That is,

$$\left.\frac{\partial \Delta p_n(x,t)}{\partial x}\right|_{x=0} = \left.\frac{J_{eo}}{q p_{no} D_p} \Delta p_n(x,t)\right|_{x=0} \tag{3.15}$$

where

$$p_{no} = \frac{n_i^2}{N_D} \tag{3.16}$$

and we have dropped the subscript notation for the base. Observe that instead of equaling zero as in the Rose-Weaver analysis, the gradient of the excess minority carrier concentration at $x = 0$ is now proportional to the excess minority carrier concentration and to the emitter component of the total saturation current.

Again, the recombination at the effective back surface of the solar cell is described completely in terms of the excess minority carrier hole concentration in the base. The boundary condition for the excess minority carrier concentration at $x = W$ for the open circuit voltage case is therefore identical to that derived for the short circuit current case,

$$\left.\frac{\partial \Delta p_n(x,t)}{\partial x}\right|_{x=W} = -\left.\frac{S_p}{D_p} \Delta p_n(x,t)\right|_{x=W}. \tag{3.17}$$

Applying the new set of boundary conditions to the general solution of the continuity equation, we derive the excess minority carrier concentration in the base under open circuit voltage conditions to be

$$\Delta p_{n_V}(x,t) = \sum_{m=1}^{\infty} C_{V_m} \cos \beta_{V_m} x \cdot \exp\left[-\left(\beta_{V_m}^2 D_p + \frac{1}{\tau_p}\right)t\right] \tag{3.18}$$

where

$$\left[\beta_{V_m} - \frac{S_p J_{eo}}{q p_{no} D_p^2 \beta_{V_m}}\right] \tan \beta_{V_m} W = \frac{S_p}{D_p} + \frac{J_{eo}}{q p_{no} D_p} \tag{3.19}$$

and

$$\frac{1}{\tau_{V_m}} = \beta_{V_m}^2 D_p + \frac{1}{\tau_p}. \tag{3.20}$$

Note that the application of Jain's open circuit voltage boundary condition results in an eigenvalue expression for β_{V_m} (Equation 3.19) which includes the emitter saturation current, J_{eo}. When emitter recombination is negligible, J_{eo}

becomes zero and Equation 3.19 reduces to the eigenvalue expression derived by Rose and Weaver,

$$\beta_{V_m} \tan \beta_{V_m} W = \frac{S_p}{D_p} . \tag{3.21}$$

3.1.2 Decay Rates

We investigate in this section the effects of emitter recombination on the decay rates of the short circuit current and the open circuit voltage.

3.1.2.1 Short Circuit Current Decay Rate

The short circuit current in the Rose-Weaver analysis was originally written in terms of the excess minority carrier concentration as

$$J_{sc}(t) = qD_p \left. \frac{\partial \Delta p_{n_J}(x,t)}{\partial x} \right|_{x=0} \tag{3.22}$$

where $\Delta p_{n_J}(x,t)$ is the excess minority carrier concentration under short circuit current conditions given in Equation 2.19. Then, evaluating the expression above, we obtained the result

$$J_{sc}(t) = \sum_{m=1}^{\infty} J_{sc_m} \exp\left[-\frac{t}{\tau_{J_m}}\right] \tag{3.23}$$

where

$$\frac{1}{\tau_{J_m}} = \beta_{J_m}^2 D_p + \frac{1}{\tau_p} \tag{3.24}$$

and

$$J_{sc_m} = qD_p C_{J_m} \beta_{J_m}. \tag{3.25}$$

To include the effect of emitter recombination, we must really write

$$J_{sc}(t) = qD_p \left. \frac{\partial \Delta p_{n_J}(x_B,t)}{\partial x_B} \right|_{x_B=0} - qD_n \left. \frac{\partial \Delta n_{p_J}(x_E,t)}{\partial x_E} \right|_{x_E=0} \tag{3.26}$$

where Δp_n is the excess minority carrier concentration in the base and Δn_p is the excess minority carrier concentration in the emitter. As stated previously,

the effect of space-charge recombination can be ignored since the junction voltage under short circuit conditions is exactly zero.

Assuming we can find the solution to the continuity equation on the emitter side of the junction, we then evaluate Equation 3.26 to find

$$J_{sc}(t) = \sum_{m=1}^{\infty} J_{sc_{B_m}} \exp\left[-\frac{t}{\tau_{J_{B_m}}}\right] + \sum_{m=1}^{\infty} J_{sc_{E_m}} \exp\left[-\frac{t}{\tau_{J_{E_m}}}\right]. \qquad (3.27)$$

In a manner similar to our argument for the quasi-static emitter approximation, we assume that for typical minority carrier lifetimes in the base and the emitter, the emitter decay rate, $\tau_{J_{E_m}}$, will be much shorter than the base decay rate, $\tau_{J_{B_m}}$. Therefore, we expect the emitter contribution to the short circuit current to decay much more rapidly than the base contribution. Thus, we are assured that, after a sufficient wait, our measurement of the short circuit current decay reflects just the decay of the minority carriers in the base. Furthermore, after a sufficient time delay, even the higher order terms in the base decay to insignificant levels, leaving just the first order term dependence. In this case, we have once again the Rose-Weaver result for the short circuit current decay rate,

$$\frac{1}{\tau_{J_1}} = \beta_{J_1}^2 D_p + \frac{1}{\tau_p}. \qquad (3.28)$$

3.1.2.2 Open Circuit Voltage Decay Rate

In the Rose-Weaver analysis, the open circuit voltage was written in terms of the minority carrier concentration through the law of the junction. That is,

$$V_{oc}(t) = n V_T \ln\left[\frac{\Delta p_{n_V}(x,t)}{p_{no}} + 1\right]\Bigg|_{x=0} \qquad (3.29)$$

where $\Delta p_{n_V}(x,t)$ is the excess minority carrier hole concentration under open circuit voltage conditions given in Equation 2.24.

By virtue of Jain's efforts, the excess minority carrier hole concentration in the base under open circuit voltage conditions now includes the effect of emitter recombination. The only difference between the Rose-Weaver result, Equation 2.24, and the Jain result, Equation 3.18, for the excess minority carrier concentration is the definition of the open circuit voltage decay eigenvalue, β_{V_m}. Thus, substituting Equation 3.18 into Equation 3.29 leads to

an expression for the open circuit voltage decay rate identical to the Rose-Weaver result,

$$\frac{1}{\tau_{V_1}} = \beta_{V_1}^2 D_p + \frac{1}{\tau_p}, \tag{3.30}$$

provided the expression for the open circuit voltage decay eigenvalue is given by

$$\left[\beta_{V_1} - \frac{S_p J_{eo}}{q p_{no} D_p^2 \beta_{V_1}}\right] \tan \beta_{V_1} W = \frac{S_p}{D_p} + \frac{J_{eo}}{q p_{no} D_p}. \tag{3.31}$$

Note that we have again assumed that a brief delay in the measurement allows all higher order decay terms to fall to negligible levels such that the fundamental term alone is significant in the asymptotic region of the decay. We also recall that the light bias technique used by Rose and Weaver places the solar cell operation far above the voltages at which space-charge recombination is important.

3.2 Rose-Weaver-Jain Model Equations

We have examined the effects of emitter and space-charge recombination on the Rose-Weaver analysis of a BSF solar cell under short circuit current and open circuit voltage decay. We find that the effect of space-charge recombination is indeed negligible. However, the effect of emitter recombination, as demonstrated by Jain, leads to a significant change in the eigenvalue equation for the open circuit voltage decay in the Rose-Weaver Model. A revised model, which incorporates Jain's analysis of the emitter recombination, is appropriately called the Rose-Weaver-Jain Model.

The Rose-Weaver-Jain Model equations are thus:

$$\beta_J \cot \beta_J W = -\frac{S_p}{D_p} \tag{3.32}$$

$$\left[\beta_V - \frac{S_p J_{eo}}{q p_{no} D_p^2 \beta_V}\right] \tan \beta_V W = \frac{S_p}{D_p} + \frac{J_{eo}}{q p_{no} D_p} \tag{3.33}$$

$$\frac{1}{\tau_J} = \beta_J^2 D_p + \frac{1}{\tau_p} \tag{3.34}$$

$$\frac{1}{\tau_V} = \beta_V^2 D_p + \frac{1}{\tau_p} \tag{3.35}$$

where

$$p_{no} = \frac{n_i^2}{N_D} . \tag{3.36}$$

Again, we drop the subscript m=1 with the understanding that only the first order term is significant in our measurements of the short circuit current and open circuit voltage decay rates.

In the Rose-Weaver-Jain Model, we measure τ_J, τ_V, W, the base resistivity, and the temperature. With the base resistivity and the temperature measurements, we refer to published data to determine n_i, D_p, and N_D. The quantities to be solved in the model are τ_p, S_p, and J_{eo}. The eigenvalues, β_J and β_V, are quantities for which we must also find solutions. Thus, we have five unknown quantities in the model. However, we presently have only four equations with which to solve for these five unknowns. Clearly, we must add one more equation to the four above in order to make the simultaneous solution of the system possible. The equation to be added is, in fact, found by including the total saturation current density, J_o, in the model.

Assuming we take measurements of J_{sc}–V_{oc} at open circuit voltages for which space-charge recombination is negligible, we can determine J_o from Equation 1.8,

$$J_o = J_{sc} \exp\left[-\frac{V_{oc}}{V_T}\right]. \tag{3.37}$$

Moreover, for negligible space-charge recombination, Equations 1.11 and 1.12 give

$$J_o = J_{bo} + J_{eo}. \tag{3.38}$$

J_{bo}, however, can be defined in terms of variables already available in the model. From Equation 1.19,

$$J_{bo} = q p_{no} \left(\frac{D_p}{\tau_p}\right)^{1/2} \left[\frac{S_p \left(\frac{\tau_p}{D_p}\right)^{1/2} + \tanh\left(\frac{W}{\sqrt{D_p \tau_p}}\right)}{1 + S_p \left(\frac{\tau_p}{D_p}\right)^{1/2} \tanh\left(\frac{W}{\sqrt{D_p \tau_p}}\right)} \right]. \tag{3.39}$$

Substituting the above expression into Equation 3.38, we derive a fifth equation for the Rose-Weaver-Jain Model,

$$J_o = J_{eo} + q p_{no} \left(\frac{D_p}{\tau_p}\right)^{1/2} \left[\frac{S_p \left(\frac{\tau_p}{D_p}\right)^{1/2} + \tanh\left(\frac{W}{\sqrt{D_p \tau_p}}\right)}{1 + S_p \left(\frac{\tau_p}{D_p}\right)^{1/2} \tanh\left(\frac{W}{\sqrt{D_p \tau_p}}\right)} \right], \tag{3.40}$$

which makes possible the simultaneous solution for τ_p,S_p, J_{eo}, β_J, and β_V.

3.3 Extending the Rose-Weaver-Jain Model

It is possible at this point to find solutions to the Rose-Weaver-Jain Model by measuring τ_J, τ_V, J_{sc}, V_{oc}, the base resistivity, and the temperature, and by using empirical data for n_i, D_p, and N_D. However, an extension of the Rose-Weaver-Jain Model removes the dependency of the solutions on the published values for n_i, D_p, and N_D. The extension, in fact, allows for the simultaneous solution of not only τ_p, S_p, and J_{eo}, but also D_p and p_{no}, where p_{no} is a function of n_i and N_D (refer to Equation 3.36).

The ability to determine τ_p, S_p, and J_{eo} independently of n_i, D_p, and N_D is very desirable since values for n_i, D_p, and N_D can be found only approximately from published data. For example, the base doping, N_D, is obtained from a measurement of the base resistivity. Although charts of the doping concentration versus resistivity exist [13], the difficulty involved in interpolating values from the logarithmic scales of these charts introduces uncertainty in the determination of N_D. The diffusion coefficient, D_p, is similarly obtained from a measurement of the base resistivity. Again, charts of the diffusion coefficient versus resistivity exist [13]. However, the same difficulties encountered in determining N_D from the resistivity charts are present for D_p. An additional difficulty in the determination of D_p is even more alarming. That is, the resistivity charts provide values for the majority carrier diffusion coefficient when, actually, it is values for the minority carrier diffusion

coefficient that we desire. Finally, the greatest source of uncertainty among the empirical parameters concerns the intrinsic carrier concentration, n_i. Checking the literature, we encounter wide discrepancies for this parameter. For example, at T = 300° K, the intrinsic carrier concentration n_i in silicon is reported in one textbook to be 1.45×10^{10} cm^{-3} [5], while a model by Barber [14] reports n_i to be 1.23×10^{10} cm^{-3}. The uncertainty in n_i is compounded by the fact that it is the square of n_i which appears in the model equations. Indeed, the ability to determine τ_p, S_p, and J_{eo} independently of n_i, D_p, and N_D is a most desirable trait of the extended model.

In the following section, we describe the experiment which makes the extension of the Rose-Weaver-Jain Model possible. The experiment requires the removal of the back surface field of the solar cell. We then indicate how the Rose-Weaver-Jain Model equations, when the back surface field is removed, take on especially simple forms and, when combined with the original model equations for which the back surface field is intact, permit the solution of a greater set of variables than possible before.

3.3.1 Back Surface Field Removal Experiment

The back surface field removal experiment, as devised by Rose and Weaver [11], requires stripping off the back ohmic contact of the solar cell, sandblasting away the back surface field, reattaching the ohmic contact, and taking the same data set as that with the back surface field intact. In the experiment, the following assumptions are made:

[1] the back surface recombination velocity of the sandblasted cell is no longer small as in the back surface field case, but is now extremely large due to the ohmic contact. We assume, in fact, that the back surface recombination velocity for the sandblasted cell is infinite.

[2] the temperature is the same in both the original and the sandblasted cell so that temperature dependent parameters such as n_i, D_p, and N_D remain constant between experiments. This assumption is particularly critical for n_i. It is known that, at room temperature, an increase in temperature of one degree Kelvin causes n_i to increase approximately ten percent [15].

[3] the sandblasting at the back of the cell does not affect the condition of the emitter. Thus, for the same temperature, we expect the emitter component, J_{eo}, of the total saturation current to be equivalent for both the original and the sandblasted cells. This assumption has in

fact been verified by Rose and Weaver by measuring the blue wavelength response in the emitter for both cases and noting the constancy of this response [11].

[4] the degradation of the minority carrier hole lifetime in the base is a possibility. It has been suggested that the sandblasting at the back of the cell may have produced small cracks extending deep into the base [11].

We now apply these assumptions to the Rose-Weaver-Jain Model. To indicate those quantities in the model whose values change (or may possibly change, as in the case of the minority carrier hole lifetime in the base) because of the back surface field removal we append the subscript r. The quantities whose values remain constant between the two experiments are unchanged in notation.

In Equation 3.32, infinite S_{p_r} forces the eigenvalue β_{J_r} to

$$\beta_{J_r} = \frac{\pi}{W_r} . \tag{3.41}$$

In Equation 3.33, infinite S_{p_r} yields

$$J_{eo} = -q p_{no} D_p \beta_{V_r} \cot \beta_{V_r} W_r . \tag{3.42}$$

The decay rate equations, Equations 3.34 and 3.35, retain their previous form, but are altered by the subscript r:

$$\frac{1}{\tau_{J_r}} = \beta_{J_r}^2 D_p + \frac{1}{\tau_{p_r}} \tag{3.43}$$

$$\frac{1}{\tau_{V_r}} = \beta_{V_r}^2 D_p + \frac{1}{\tau_{p_r}} . \tag{3.44}$$

Finally, infinite S_{p_r} in Equation 3.40 results in the simplification

$$J_{o_r} = J_{eo} + q p_{no} \left(\frac{D_p}{\tau_{p_r}} \right)^{1/2} \coth \frac{W_r}{\sqrt{D_p \tau_{p_r}}} \tag{3.45}$$

where

$$J_{o_r} = J_{sc_r} \exp \left(- \frac{V_{oc_r}}{V_T} \right) . \tag{3.46}$$

3.3.2 Combining the BSF and the BSF Removal Experiments

The assumptions of the back surface field removal experiment greatly simplify the Rose-Weaver-Jain Model Equations. Specifically, the assumption of infinite surface recombination velocity at the back of the sandblasted cell removes S_{p_r} from the model equations and reduces the solution variable, β_{J_r}, to a fixed value. Thus, when these model equations are combined with the model equations of the original experiment, the total number of equations exceeds the total number of solution variables. We are therefore permitted to designate quantities, whose values were previously determined by empirical data, to be solution variables. In fact, we will show that it is possible to solve not only for τ_p, S_p, and J_{eo}, but also for τ_{p_r}, D_p, and p_{no}. In this manner, we remove model dependency on published values of n_i, D_p, and N_D to obtain more accurate solutions for τ_p, S_p, and J_{eo}. Indeed, the method provides a way to experimentally determine D_p, p_{no}, and τ_{p_r}.

In Chapter IV, we describe in detail how the model equations for the two experiments are combined into one simultaneous system of equations and the solutions found using the Purdue University Computing Center library subroutine, SECANT [16].

CHAPTER IV
SIMULTANEOUS NUMERICAL SOLUTION OF THE COMBINED MODEL

In Chapter II, we assumed that the recombination of minority carriers in the BSF solar cell is base dominated. Under this assumption, knowledge of τ_p and S_p completely characterizes the recombination in the cell. We then presented the Rose-Weaver Method, an experimental technique permitting the determination of τ_p and S_p in the base dominated BSF solar cell. We also presented the model derived by Rose and Weaver in the course of their analysis.

In Chapter III, however, we discussed various studies which indicate that recombination in the emitter can form a significant component of the total cell recombination. Consequently, we presented an analysis of the emitter recombination by Jain which demonstrates that the determination of τ_p, S_p, and J_{eo} is necessary in order to fully describe recombination in the BSF solar cell.

In an attempt to remove the dependency of the solutions for τ_p, S_p, and J_{eo} on published values for n_i, D_p, and N_D, we discussed at the end of Chapter III an extension of the Rose-Weaver-Jain Model. The extension of the model requires the removal of the back surface field of the solar cell. When the back surface field is removed, the Rose-Weaver-Jain Model equations are greatly simplified. We then concluded Chapter III by indicating that the model equations derived for the two conditions of the back surface field (back surface field intact and back surface field removed) can be combined into one large system which can be solved simultaneously for τ_p, τ_{p_r}, S_p, J_{eo}, D_p, and p_{no}.

In this chapter, we perform the steps necessary to combine the model equations derived from the two conditions of the back surface field into a system of simultaneous equations in τ_p, τ_{p_r}, S_p, J_{eo}, D_p, and p_{no}. For convenience, this system of simultaneous equations is called the Combined Rose-Weaver-Jain Model or, for short, the Combined Model. A program utilizing the Purdue University Computing Center (PUCC) subroutine,

SECANT [16], is then written to find solutions to the Combined Model. As a test of our solution procedure, we consider a set of measurements taken by Rose and Weaver on three BSF solar cells fabricated by Sandia National Laboratories.

Our inability to find a simultaneous solution to the Combined Model for any of the Sandia cells prompts us to investigate the sensitivity of the solution, when the solution is known to exist, to small uncertainties in the experimental measurements. An analysis of the sensitivity is performed for the Combined Model and the results reveal that extremely large variations in the solution occur for even slight perturbations in the experimental measurements. Believing the complexity of the Combined Model to be responsible for the large variations in the solution, we return to the Rose-Weaver-Jain Model, which is considerably less complex than the Combined Model, and examine its sensitivities. While the Rose-Weaver-Jain Model exhibits smaller variations in the solution to uncertainties in the experimental measurements, the need to know precise values for the empirical parameters, especially n_i, becomes critical.

At first, it was believed that the insensitivity of the solution to experimental measurement merely indicates that the description of the cell recombination itself is insensitive to exact knowledge of the solution. A careful study of the integrated recombination using the solar cell analysis program SCAP1D [17], however, disproves this hypothesis. Instead, the results of SCAP1D provide confirmation that small uncertainties in the experimental measurements and the empirical parameters can lead to radically different interpretations of recombination in the solar cell.

4.1 Constructing a System of Simultaneous Equations

Our first task is to write the combined set of Rose-Weaver-Jain Model equations into a system of simultaneous equations. We begin by listing the Rose-Weaver-Jain Model equations, first with the back surface field intact, then with the back surface field removed.

With the back surface field intact:

$$\beta_J \cot \beta_J W = -\frac{S_p}{D_p} \tag{4.1}$$

$$\left[\beta_V - \frac{S_p J_{eo}}{q p_{no} D_p^2 \beta_V}\right] \tan \beta_V W = \frac{S_p}{D_p} + \frac{J_{eo}}{q p_{no} D_p} \tag{4.2}$$

$$\frac{1}{\tau_J} = \beta_J^2 D_p + \frac{1}{\tau_p} \tag{4.3}$$

$$\frac{1}{\tau_V} = \beta_V^2 D_p + \frac{1}{\tau_p} \tag{4.4}$$

$$J_o = J_{eo} + q p_{no} \left(\frac{D_p}{\tau_p}\right)^{1/2} \left[\frac{S_p \left(\frac{\tau_p}{D_p}\right)^{1/2} + \tanh\left(\frac{W}{\sqrt{D_p \tau_p}}\right)}{1 + S_p \left(\frac{\tau_p}{D_p}\right)^{1/2} \tanh\left(\frac{W}{\sqrt{D_p \tau_p}}\right)}\right]. \tag{4.5}$$

With the back surface field removed:

$$\beta_{J_r} = \frac{\pi}{W_r} \tag{4.6}$$

$$J_{eo} = -q p_{no} D_p \beta_{V_r} \cot \beta_{V_r} W_r \tag{4.7}$$

$$\frac{1}{\tau_{J_r}} = \beta_{J_r}^2 D_p + \frac{1}{\tau_{p_r}} \tag{4.8}$$

$$\frac{1}{\tau_{V_r}} = \beta_{V_r}^2 D_p + \frac{1}{\tau_{p_r}} \tag{4.9}$$

$$J_{o_r} = J_{eo} + q p_{no} \left(\frac{D_p}{\tau_{p_r}}\right)^{1/2} \coth \frac{W_r}{\sqrt{D_p \tau_{p_r}}}. \tag{4.10}$$

In the equations above, τ_J, τ_V, J_o, W, τ_{J_r}, τ_{V_r}, J_{o_r}, and W_r represent eight independent measurements on the solar cell. Thus, the total number of independent output variables which can be solved for simultaneously is eight. Similarly, the total number of independent equations which must be written for the system is eight. Presently, the number of equations in the system is ten. As we shall see, two of these equations are dependent. For example, in Equation 4.6, β_{J_r} is known directly from an experimental measurement of W_r.

Thus, Equation 4.6 can be eliminated by substitution into the rest of system. Also, Equation 4.7 for J_{eo} can then be eliminated by substitution into the rest of the system.

The Combined Model equations are thus:

$$\beta_J \cot \beta_J W = -\frac{S_p}{D_p} \tag{4.11}$$

$$\left[\beta_V + \frac{S_p \beta_{V_r} \cot \beta_{V_r} W_r}{D_p \beta_V}\right] \tan \beta_V W = \frac{S_p}{D_p} - \beta_{V_r} \cot \beta_{V_r} W_r \tag{4.12}$$

$$\frac{1}{\tau_J} = \beta_J^2 D_p + \frac{1}{\tau_p} \tag{4.13}$$

$$\frac{1}{\tau_V} = \beta_V^2 D_p + \frac{1}{\tau_p} \tag{4.14}$$

$$J_o = -q\, p_{no} D_p \beta_{V_r} \cot \beta_{V_r} W_r + q\, p_{no} \left(\frac{D_p}{\tau_p}\right)^{1/2} \left[\frac{S_p \left(\frac{\tau_p}{D_p}\right)^{1/2} + \tanh\left(\frac{W}{\sqrt{D_p \tau_p}}\right)}{1 + S_p \left(\frac{\tau_p}{D_p}\right)^{1/2} \tanh\left(\frac{W}{\sqrt{D_p \tau_p}}\right)}\right] \tag{4.15}$$

$$\frac{1}{\tau_{J_r}} = \left(\frac{\pi}{W_r}\right)^2 D_p + \frac{1}{\tau_{p_r}} \tag{4.16}$$

$$\frac{1}{\tau_{V_r}} = \beta_{V_r}^2 D_p + \frac{1}{\tau_{p_r}} \tag{4.17}$$

$$J_{o_r} = -q\,p_{no}\,D_p\,\beta_{V_r}\cot\beta_{V_r}W_r + q\,p_{no}\left(\frac{D_p}{\tau_{p_r}}\right)^{1/2}\coth\frac{W_r}{\sqrt{D_p\tau_{p_r}}}\,. \tag{4.18}$$

The eight independent solution variables are β_J, β_V, D_p, S_p, τ_p, p_{no}, β_{V_r}, and τ_{p_r}; while the dependent solution variable J_{eo} can be found from

$$J_{eo} = -q\,p_{no}\,D_p\,\beta_{V_r}\cot\beta_{V_r}W_r\,. \tag{4.19}$$

Observe that our solution is independent of n_i and N_D. In fact, the solution of the system for p_{no}, where

$$p_{no} = \frac{n_i^2}{N_D}\,, \tag{4.20}$$

provides a means of calculating n_i given our knowledge of N_D from the base resistivity.

4.2 SECANT

We have written a Fortran program to solve the system of equations which comprise the Combined Model. To handle the nonlinearities present in the system, we find the PUCC subroutine SECANT particularly useful [16]. The Fortran program and a discussion of our use of SECANT appears in Appendix C.

4.3 Results of the Simultaneous Numerical Solution

To test the utility of our program, we examine a set of three 0.3 ohm-cm P^+NN^+ Sandia solar cells for which Rose and Weaver have performed measurements of the short circuit current and the open circuit voltage decay rates [11]. Measurements for both the back surface field (BSF) case and the case in which the back surface field has been removed (BSF Removed) are reported in Table 4.1.

We assume, as is necessary for simultaneous solution, that the BSF and BSF Removed experiments are performed at precisely the same temperature. From the reference we infer that the measurement temperature was 25°C. Measurements of the open circuit voltage and the short circuit current, also recorded in Table 4.1, can then be used along with our knowledge of the

Table 4.1 Rose-Weaver Measurements on three 0.3 ohm-cm P^+NN^+ Sandia Solar Cells [11]

Cell	BSF				BSF Removed			
	V_{oc} (mV)	J_{sc} (mA-cm^{-2})	τ_J (μsec)	τ_V (μsec)	V_{oc_r} (mV)	J_{sc_r} (mA-cm^{-2})	τ_{J_r} (μsec)	τ_{J_r} (μsec)
1	640	24.4	39.4	72.9	631	24.3	23.9	47.1
2	642	24.4	37.3	78.0	627	24.2	21.9	46.9
3	643	24.8	39.3	79.0	630	24.6	24.2	50.2

thermal voltage to calculate the total saturation current from

$$J_o = J_{sc} \exp\left[-\frac{V_{oc}}{V_T}\right] \tag{4.21}$$

and

$$J_{o_r} = J_{sc_r} \exp\left[-\frac{V_{oc_r}}{V_T}\right]. \tag{4.22}$$

Also, in the reference, we find the width of the BSF cell to be 533 microns. Sandblasting off the BSF, it is reported, removes approximately ten microns from the back of the cell. Thus, we assume the width of the sandblasted cell to be 523 microns.

We have now assembled values for the eight independent inputs necessary to solve the Combined Model by the SECANT Method. We summarize these inputs in Table 4.2.

Providing an initial guess for the solution such as the one proposed in Appendix C, we run our program.

Despite changing the initial guess to the solution, we can not find a solution for any of the three cells in the set. Such results prompt us to question:

[1] the reliability of our program. More specifically, can SECANT find the solution to a system of simultaneous equations when a solution is indeed known to exist?

[2] the consistency of the Rose-Weaver experiment. That is, has the experiment been carefully controlled? Recall that the maintenance of constant temperature between the BSF and BSF Removed experiments is essential if we are to assume D_p, n_i, and N_D are the same in each experiment.

[3] the completeness of the model equations. Perhaps, we have left out some important physical effect.

Assuming that a tight temperature control has been maintained between the BSF and BSF Removed experiments and that the Combined Model correctly describes the physics of the short circuit current and the open circuit voltage decay, we examine the first question in detail. To answer this question, we devise a simple test. We begin the test by assuming we know a solution to the system of simultaneous equations. From the system equations, we then calculate the "measurements" required for the assumed solution. Using these

Table 4.2 Input Data for the Combined Model

Cell	BSF				BSF Removed			
	τ_J (μsec)	τ_V (μsec)	J_o (10^{-15}A-cm^{-2})	W (μm)	τ_{J_r} (μsec)	τ_{V_r} (μsec)	J_{o_r} (10^{-15}A-cm^{-2})	W_r (μm)
1	39.4	72.9	379.0	533.0	23.9	47.1	535.5	523.0
2	37.3	78.0	350.6	533.0	21.9	46.9	623.1	523.0
3	39.3	79.0	342.8	533.0	24.2	50.2	563.4	523.0

"measurements" as input to the Combined Model, we then run SECANT to verify whether it does indeed return the assumed solution.

A test of the numerical ability of SECANT, as described above, has been performed. The results reveal that SECANT has no difficulty in solving the Combined Model, given a reasonable initial guess to the solution. The results thus give us a self-consistent set of measurements and solutions for the Combined Model.

Having proven that solutions to the Combined Model can be found, it becomes evident that this simple experiment to test the numerical capability of SECANT can be extended to study the sensitivity of the solution to small perturbations in the experimental data.

4.4 Sensitivity Analysis

A study of the sensitivity of the solution to small perturbations in the experimental data begins with the self-consistent set of "measurements" and solutions described in the preceding section. The measurements necessary to render the assumed solution are known as the "baseline" set of measurements. By perturbing the "measured values," one at a time, from the baseline set, we then determine from our program the new solution to the system. This technique thus provides a means of studying the variations in the solution to the small uncertainties which inevitably occur in experimental measurement.

The analysis of the sensitivity is performed first for the Combined Model, which has been the focus of our efforts thus far. Since the measurement precision required for this model is found to be prohibitively strict, we consequently return to the Rose-Weaver-Jain Model, or BSF Model, to determine whether the measurement precision required for this simpler model is more favorable for experiment. While the BSF Model shows improved sensitivity to the measurements of the asymptotic decay rates and the total saturation current, the determination of correct solutions to the model are now complicated by the need to accurately infer D_p, N_D, and n_i from empirical data.

4.4.1 The Combined Model

To form the baseline set of measurements for the Combined Model, we assume that the following parameter values are typical for a high quality silicon solar cell:

$$\tau_p = 300.0 \times 10^{-6} \text{ sec}$$

$$S_p = 500.0 \text{ cm–sec}^{-1}$$

$$J_{eo} = 150.0 \times 10^{-15} \text{ amps–cm}^{-2}$$

$$W = 533.0 \times 10^{-4} \text{ cm}$$

$$D_p = 10.0 \text{ cm}^2\text{–sec}^{-1}$$

$$n_i = 1.20 \times 10^{10} \text{ cm}^{-3}$$

$$N_D = 2.0 \times 10^{16} \text{ cm}^{-3}.$$

We also assume that after the back surface field removal:

$$\tau_r = 200.0 \times 10^{-6} \text{ sec}$$

$$W_r = 523.0 \times 10^{-4} \text{ cm}.$$

According to our definitions, the parameters chosen above represent a mixture of experimental measurements, independent solution variables, dependent solution variables, and empirical data. However, from the values of these parameters, it is possible to solve for the "measurements" and solutions in the Combined Model. We can therefore use the set of parameters above to determine the baseline set of "measurements" (and the solutions which correspond to this baseline set) in the Combined Model. In Table 4.3 we present the baseline set of "measurements" and the values for the independent and dependent solution variables which result from our choice of typical parameter values for a high quality solar cell.

We now fluctuate the measurement values, one at a time, from the baseline set. The range of the fluctuation is $\pm$ 3 %. With our program, we can study the effect of the fluctuation on the solution. The independent solution variables are S_p, D_p, p_{no}, L_p, L_{p_r}, β_V, β_J, and β_{V_r}. The eigenvalues, β_J, β_V, and β_{V_r}, are auxiliary variables to the solution and are not of interest in the sensitivity analysis. Also, we are not interested in the diffusion lengths themselves, but in the minority carrier lifetimes, τ_p and τ_{p_r}, which can be derived through the diffusion length definition. We can likewise calculate J_{eo} from the independent solutions through Equation 4.19 and therefore observe the response of this parameter to the fluctuation. Finally, if we assume that N_D is accurately known from the base resistivity, we can use the solution for

Table 4.3 Baseline Set for the Combined Model

Measurements	Solutions
τ_J = 42.1454 μsec	β_J = 45.160 cm^{-1}
τ_V = 89.3249 μsec	β_V = 28.039 cm^{-1}
J_o = 390.249 $\times$ 10^{-15} A–cm^{-2}	β_{V_r} = 36.574 cm^{-1}
W = 533.0 μm	D_p = 10.0 cm^2–sec^{-1}
τ_{J_r} = 24.3413 μsec	S_p = 500.0 cm–sec^{-1}
τ_{V_r} = 54.4172 μsec	p_{no} = 7.2 $\times$ 10^3 cm^{-3}
J_{o_r} = 462.577 $\times$ 10^{-15} A–cm^{-2}	L_p = 547.732 μm
W_r = 523.0 μm	L_{p_r} = 447.219 μm
Empirical Parameter	**Dependent Solutions**
N_D = 2.0 $\times$ 10^{16} cm^{-3}	τ_p = 300.0 μsec
	τ_{p_r} = 200.0 μsec
	J_{eo} = 150.0 $\times$ 10^{-15} A–cm^{-2}
	n_i = 1.20 $\times$ 10^{10} cm^{-3}

p_{no} to study the fluctuation in n_i. Thus, in the analysis, we shall find the sensitivities of τ_p, S_p, J_{eo}, τ_{p_r}, n_i, and D_p to the fluctuations in the experimental measurements.

The results of the sensitivity analysis are recorded in Tables 4.4 to 4.11. We have created a table for each of the eight independent measurements in the Combined Model. These eight measurements, we recall, are τ_J, τ_V, J_o, W, τ_{J_r}, τ_{V_r}, J_{o_r}, and W_r. In the left-most column of each table we record the values of the measured quantity we have chosen to fluctuate. We also indicate in this column the percent change of these values from the baseline value. In the columns to the right we report the variation in value of the solution variables whose response to fluctuations in the measured quantity we have chosen to study. Again, we include the percent change of these values from the baseline value.

The tables demonstrate quite clearly the large variation in value of the solutions, in particular, τ_p, S_p, J_{eo}, and τ_{p_r}, to small fluctuations in the experimental measurements. Perhaps the most prominent feature of the tables is that, for a fluctuation of only $+3$ % in τ_V, J_o, or W_r, or of only -3 % in τ_{V_r} or J_{o_r}, no solution is possible. Furthermore, it is observed from the tables that a measurement precision of ± 1 % can, at best, determine τ_p within -6.4 %, S_p within -6.7 %, J_{eo} within 3.2 %, and τ_{p_r} within -4.3 %. At worst, a measurement precision of ± 1% leads to variations in τ_p of 56.2 %, in S_p of 10.6 %, in J_{eo} of -23.0 %, and in τ_{p_r} of 44.8 %. The variation of n_i and D_p in response to a measurement precision of ± 1% is not nearly as extreme. A typical value of this variation is ± 3 %. Finally, note that the variation of the solutions increases monotonically with decreasing precision of the experimental data. More importantly, note that we have not considered as yet the more likely case of uncertainty in all the measurements at once.

In conclusion, it is quite evident that meticulous care must be taken to reduce experimental error to very small levels in order to use the Rose-Weaver Method as a means of extracting detailed information on recombination in the BSF solar cell. Presently, Rose and Weaver report about five percent accuracy in their measurements of the short circuit and open circuit voltage decay rates [11].

Believing the complexity of the Combined Model to be responsible for the poor sensitivities, we now decide to examine the sensitivities of the BSF Model, which can be written as a system of five simultaneous equations.

Table 4.4 Combined Model: τ_J Fluctuation

Measurement		Solution											
τ_J (μsec)	$\Delta\tau_J$ (%)	τ_p (μsec)	$\Delta\tau_p$ (%)	S_p (cm$-$sec^{-1})	ΔS_p (%)	$J_{eo}(\times 10^{-15})$ (A$-$cm^{-2})	ΔJ_{eo} (%)	τ_{pr} (μsec)	$\Delta\tau_{pr}$ (%)	$n_i(\times 10^{10})$ (cm^{-3})	Δn_i (%)	D_p (cm$^2-$sec^{-1})	ΔD_p (%)
40.8810	-3.0	1520.8	406.9	679.6	35.9	214.5	43.0	488.0	144.0	1.13	-5.6	10.82	8.2
41.3025	-2.0	614.7	104.9	612.6	22.5	192.0	28.0	320.6	60.3	1.16	-3.6	10.52	5.2
41.7239	-1.0	397.6	32.5	553.1	10.6	170.5	13.7	244.0	22.0	1.18	-1.8	10.25	2.5
42.1454	0.0	300.0	0.0	500.0	0.0	150.0	0.0	200.0	0.0	1.20	0.0	10.00	0.0
42.5669	1.0	244.5	-18.5	452.4	-9.5	130.4	-13.0	171.4	-14.3	1.22	1.7	9.77	-2.3
42.9883	2.0	208.6	-30.5	409.5	-18.1	111.7	-25.5	151.3	-24.3	1.24	3.3	9.55	-4.5
43.4098	3.0	183.6	-38.8	370.6	-25.9	93.8	-37.5	136.5	-31.8	1.26	4.8	9.35	-6.5

Table 4.5 Combined Model: τ_V Fluctuation

Measurement		Solutions											
τ_V (μsec)	$\Delta\tau_V$ (%)	τ_p (μsec)	$\Delta\tau_p$ (%)	S_p (cm-sec^{-1})	ΔS_p (%)	J_{eo}($\times 10^{-15}$) (A-cm^{-2})	ΔJ_{eo} (%)	τ_{pr} (μsec)	$\Delta\tau_{pr}$ (%)	n_i($\times 10^{10}$) (cm^{-3})	Δn_i (%)	D_p (cm^2-sec^{-1})	ΔD_p (%)
86.6452	-3.0	150.6	-49.8	371.5	-25.7	54.4	-63.7	113.1	-43.5	1.30	8.2	8.93	-10.7
87.5384	-2.0	179.2	-40.3	411.6	-17.7	86.3	-42.4	179.2	-34.4	1.27	5.4	9.27	-7.3
88.4317	-1.0	223.2	-25.6	454.3	-9.1	118.2	-21.2	157.7	-21.2	1.23	2.7	9.63	-3.7
89.3249	0.0	300.0	0.0	500.0	0.0	150.0	0.0	200.0	0.0	1.20	0.0	10.00	0.0
90.2181	1.0	468.5	56.2	548.9	9.8	181.8	21.2	278.8	39.4	1.17	-2.7	10.39	3.9
91.1114	2.0	1140.9	280.3	601.4	20.3	213.6	42.4	477.8	138.9	1.13	-5.5	10.81	8.1
92.0046	3.0	No convergence											

Table 4.6 Combined Model: J_o Fluctuation

Measurement		Solutions											
$J_o(\times 10^{-15})$ (A–cm^{-2})	ΔJ_o (%)	τ_p (μsec)	$\Delta\tau_p$ (%)	S_p (cm–sec^{-1})	ΔS_p (%)	$J_{eo}(\times 10^{-15})$ (A–cm^{-2})	ΔJ_{eo} (%)	τ_{pr} (μsec)	$\Delta\tau_{pr}$ (%)	$n_i(\times 10^{10})$ (cm^{-3})	Δn_i (%)	D_p (cm^2–sec^{-1})	ΔD_p (%)
378.5415	-3.0	157.9	-47.4	398.4	-20.3	45.5	-69.7	109.0	-45.5	1.31	8.9	8.84	-11.6
382.440	-2.0	186.2	-37.9	430.8	-13.8	80.6	-46.3	127.5	-36.3	1.27	5.9	9.21	-7.9
386.3465	-1.0	228.7	-23.8	464.6	-7.1	115.4	-23.0	154.9	-22.6	1.24	3.0	9.60	-4.0
390.2490	0.0	300.0	0.0	500.0	0.0	150.0	0.0	200.0	0.0	1.20	0.0	10.00	0.0
394.1515	1.0	445.0	48.3	537.2	7.4	184.3	22.9	288.2	44.1	1.16	-3.0	10.42	4.2
398.0540	2.0	902.3	200.8	576.5	15.3	218.5	45.7	538.7	169.3	1.13	-5.9	10.87	8.7
401.9565	3.0	No convergence											

Table 4.7 Combined Model: W Fluctuation

Measurement		Solutions											
W (μm)	ΔW (%)	τ_p (μsec)	$\Delta\tau_p$ (%)	S_p (cm-sec^{-1})	ΔS_p (%)	J_{eo}($\times 10^{-15}$) (A-cm^{-2})	ΔJ_{eo} (%)	τ_{pr} (μsec)	$\Delta\tau_{pr}$ (%)	n_i($\times 10^{10}$) (cm^{-3})	Δn_i (%)	D_p (cm^2-sec^{-1})	ΔD_p (%)
517.01	-3.0	245.5	-18.2	404.5	-19.1	133.0	-11.3	174.7	-12.7	1.217	1.5	9.80	-2.0
522.34	-2.0	262.5	-12.5	434.8	-13.0	139.1	-7.3	182.9	-8.5	1.211	0.9	9.87	-1.3
527.67	-1.0	280.7	-6.4	466.6	-6.7	144.8	-3.5	191.4	-4.3	1.205	0.4	9.94	-0.6
533.00	0.0	300.0	0.0	500.0	0.0	150.0	0.0	200.0	0.0	1.200	0.0	10.00	0.0
538.33	1.0	320.5	6.8	535.2	7.0	154.8	3.2	208.8	4.4	1.195	-0.4	10.06	0.6
543.66	2.0	342.2	14.1	572.3	14.5	159.3	6.2	217.6	8.8	1.190	-0.8	10.11	1.1
548.99	3.0	365.0	21.7	611.7	22.3	163.3	8.9	226.4	13.2	1.186	-1.1	10.16	1.6

Table 4.8 Combined Model: τ_{J_r} Fluctuation

Measurement		Solutions											
τ_{J_r} (μsec)	$\Delta\tau_{J_r}$ (%)	τ_p (μsec)	$\Delta\tau_p$ (%)	S_p (cm−sec^{-1})	ΔS_p (%)	$J_{eo}(\times 10^{-15})$ (A−cm^{-2})	ΔJ_{eo} (%)	τ_{pr} (μsec)	$\Delta\tau_{pr}$ (%)	$n_i(\times 10^{10})$ (cm^{-3})	Δn_i (%)	D_p (cm^2−sec^{-1})	ΔD_p (%)
23.611	-3.0	191.5	-36.2	390.6	-21.9	93.2	-37.9	145.4	-27.3	1.25	4.3	9.83	-1.7
23.8545	-2.0	216.8	-27.7	424.5	-15.1	112.1	-25.2	159.5	-20.3	1.23	2.9	9.88	-1.2
24.0979	-1.0	251.1	-16.3	460.8	-7.8	131.0	-12.6	177.1	-11.5	1.22	1.5	9.94	-0.6
24.3413	0.0	300.0	0.0	500.0	0.0	150.0	0.0	200.0	0.0	1.20	0.0	10.00	0.0
24.5847	1.0	376.0	25.3	542.4	8.5	169.0	12.7	231.1	15.5	1.18	-1.5	10.07	0.7
24.8281	2.0	510.5	70.2	588.5	17.7	188.1	25.4	275.8	37.9	1.16	-3.1	10.16	1.6
25.0715	3.0	815.3	171.7	638.9	27.8	207.4	38.2	345.8	72.9	1.14	-4.7	10.25	2.5

Table 4.9 Combined Model: τ_{V_r} Fluctuation

Measurement		Solutions											
τ_{V_r} (μsec)	$\Delta\tau_{V_r}$ (%)	τ_p (μsec)	$\Delta\tau_p$ (%)	S_p (cm–sec^{-1})	ΔS_p (%)	$J_{eo}(\times 10^{-15})$ (A–cm^{-2})	ΔJ_{eo} (%)	τ_{pr} (μsec)	$\Delta\tau_{pr}$ (%)	$n_i(\times 10^{10})$ (cm^{-3})	Δn_i (%)	D_p (cm^2–sec^{-1})	ΔD_p (%)
52.7847	-3.0	No Convergence											
53.3289	-2.0	856.5	188.5	593.9	18.8	211.4	40.9	385.6	92.8	1.13	-6.1	10.67	6.7
53.8730	-1.0	437.3	45.8	544.8	8.9	180.7	20.5	260.4	30.2	1.16	-3.0	10.32	3.2
54.4172	0.0	300.0	0.0	500.0	0.0	150.0	0.0	200.0	0.0	1.20	0.0	10.00	0.0
54.9614	1.0	231.7	-22.8	459.0	-8.2	119.2	-20.6	164.4	-17.8	1.24	3.0	9.70	-3.0
55.5055	2.0	190.7	-36.4	421.4	-15.7	88.2	-41.2	140.8	-29.6	1.27	5.9	9.42	-5.8
56.0497	3.0	163.3	-45.6	386.6	-22.7	57.2	-61.9	124.1	-38.0	1.31	9.2	9.15	-8.5

Table 4.10 Combined Model: J_{o_r} Fluctuation

Measurement		Solutions											
$J_{o_r}(\times 10^{-15})$ ($A-cm^{-2}$)	ΔJ_{o_r} (%)	τ_p (μsec)	$\Delta\tau_p$ (%)	S_p ($cm-sec^{-1}$)	ΔS_p (%)	$J_{eo}(\times 10^{-15})$ ($A-cm^{-2}$)	ΔJ_{eo} (%)	τ_{pr} (μsec)	$\Delta\tau_{pr}$ (%)	$n_i(\times 10^{10})$ (cm^{-3})	Δn_i (%)	D_p (cm^2-sec^{-1})	ΔD_p (%)
448.6997	-3.0	No Convergence											
453.3255	-2.0	942.9	214.3	578.1	15.6	215.5	43.7	559.1	179.5	1.116	-7.0	10.89	8.90
457.9512	-1.0	447.2	49.1	537.6	7.5	182.8	21.9	289.5	44.8	1.158	-3.5	10.43	4.28
462.5770	0.0	300.0	0.0	500.0	0.0	150.0	0.0	200.0	0.0	1.200	0.0	10.00	0.0
467.2028	1.0	229.2	-23.6	464.9	-7.0	116.9	-22.0	155.2	-22.4	1.241	3.4	9.60	-4.0
471.8285	2.0	187.6	-37.5	432.1	-13.6	83.6	-44.3	128.3	-35.8	1.282	6.9	9.23	-7.7
476.4543	3.0	160.0	-46.7	401.2	-19.8	50.0	-66.7	110.3	-44.9	1.320	10.0	8.87	-11.3

Table 4.11 Combined Model: W_r Fluctuation

Measurement		Solutions											
W (μm)	ΔW (%)	τ_p (μsec)	$\Delta\tau_p$ (%)	S_p (cm-sec^{-1})	ΔS_p (%)	J_{∞}($\times 10^{-15}$) (A-cm^{-2})	ΔJ_{∞} (%)	τ_{pr} (μsec)	$\Delta\tau_{pr}$ (%)	n_i($\times 10^{10}$) (cm^{-3})	Δn_i (%)	D_p (cm^2-sec^{-1})	ΔD_p (%)
507.31	-3.0	176.6	-41.1	399.4	-20.1	74.5	-50.4	136.8	-31.6	1.284	7.0	9.36	-6.4
512.54	-2.0	201.0	-33.0	428.2	-14.4	97.9	-34.8	150.7	-24.6	1.258	4.9	9.55	-4.5
517.77	-1.0	237.6	-20.8	461.2	-7.8	122.9	-18.1	170.3	-14.9	1.231	2.6	9.76	-2.4
523.00	0.0	300.0	0.0	500.0	0.0	150.0	0.0	200.0	0.0	1.200	0.0	10.00	0.0
528.23	1.0	432.5	44.1	546.7	9.3	179.8	19.9	251.5	25.8	1.166	-2.9	10.28	2.8
533.46	2.0	924.9	208.3	605.1	21.0	213.3	42.2	365.9	82.9	1.126	-6.1	10.63	6.3
538.69	3.0	No Convergence											

4.4.2 The BSF Model

As we did for the Combined Model, we can write a Fortran program featuring SECANT for the BSF Model in order to study the sensitivity of the solutions to small perturbations in the experimental measurements. The model equations for the solar cell when the back surface field is intact are given in Equations 4.1 to 4.5. The order of the system is five. The five independent measurements of the system are τ_J, τ_V, J_o, W, and the base resistivity. β_J, β_V, S_p, J_{eo}, and L_p are the five independent solution variables. τ_p is the lone dependent solution variable. To actually obtain solutions for the system we must infer values for n_i, N_D, and D_p from empirical data.

As before, we begin by assuming that the following values are typical for a high quality solar cell:

$$\tau_p = 300.0 \times 10^{-6} \text{ sec}$$

$$S_p = 500.0 \text{ cm–sec}^{-1}$$

$$J_{eo} = 150.0 \times 10^{-15} \text{ amps–cm}^{-2}$$

$$D_p = 10.0 \text{ cm}^2\text{–sec}^{-1}$$

$$n_i = 1.20 \times 10^{10} \text{ cm}^{-3}$$

$$N_D = 2.0 \times 10^{16} \text{ cm}^{-3}$$

$$W = 533.0 \times 10^{-4} \text{ cm.}$$

From the values of these parameters we solve for the "measurements" and solutions in the BSF Model. To summarize, we present in Table 4.12 the baseline set of "measurements" and the values for the independent and dependent solution variables which result from our choice of typical parameter values for a high quality solar cell. In Tables 4.13 to 4.16, we then record the sensitivity of τ_p, S_p, and J_{eo} (once again, the sensitivities of β_J and β_V are not of interest, and L_p is replaced in favor of τ_p) to fluctuations in the measurements of τ_J, τ_V, J_o, and W.

While these tables again demonstrate the large variation in value of the solutions to small perturbations in the experimental measurements, we note that the BSF Model shows an improved sensitivity to experimental measurement of τ_J, τ_V, J_o, and W when compared with the Combined Model. For example, we now find that convergent solutions are possible for

Table 4.12 Baseline Set for the BSF Model

Measurements	Solutions
$\tau_J = 42.1454\ \mu sec$	$\beta_J = 45.160\ cm^{-1}$
$\tau_V = 89.3249\ \mu sec$	$\beta_V = 28.039\ cm^{-1}$
$J_o = 390.249 \times 10^{-15}\ A\text{-}cm^{-2}$	$L_p = 547.72\ \mu m$
$W = 333.0\ \mu m$	$S_p = 500.0\ cm\text{-}sec^{-1}$
$\rho = 0.3\ ohm\text{-}cm$	$J_{eo} = 150.0 \times 10^{-15}\ A\text{-}cm^{-2}$
Empirical Parameters	**Dependent Solutions**
$n_i = 1.20 \times 10^{10}\ cm^{-3}$	$\tau_p = 300.0\ \mu sec$
$N_D = 2.0 \times 10^{16}\ cm^{-3}$	
$D_p = 10.0\ cm^2\text{-}sec^{-1}$	

Table 4.13 BSF Model: τ_J Fluctuation

Measurement		Solutions					
τ_J (μsec)	$\Delta\tau_J$ (%)	τ_p (μsec)	$\Delta\tau_p$ (%)	S_p (cm−sec^{-1})	ΔS_p (%)	$J_\infty(\times 10^{-15})$ (A−cm^{-2})	ΔJ_∞ (%)
40.0381	-5.0	590.8	96.9	753.3	50.7	176.2	17.5
40.4596	-4.0	493.7	64.6	692.3	38.5	170.9	13.9
40.8810	-3.0	424.5	41.5	637.3	27.5	165.6	10.4
41.3025	-2.0	372.6	24.2	587.4	17.5	160.4	6.9
41.7239	-1.0	332.3	10.8	541.8	8.4	155.2	3.4
42.1454	0.0	300.0	0.0	500.0	0.0	150.0	0.0
42.5669	1.0	273.6	-8.8	461.5	-7.7	144.9	-3.4
42.9883	2.0	251.5	-16.2	425.7	-14.9	139.8	-6.8
43.4098	3.0	232.8	-22.4	392.6	-21.5	134.7	-10.2
43.8312	4.0	216.7	-27.8	361.6	-27.7	129.7	-13.5
44.2527	5.0	202.7	-32.4	332.6	-33.5	124.7	-16.9

Table 4.14 BSF Model: τ_V Fluctuation

Measurement		Solutions					
τ_V (μsec)	$\Delta\tau_V$ (%)	τ_p (μsec)	$\Delta\tau_p$ (%)	S_p ($cm-sec^{-1}$)	ΔS_p (%)	$J_{eo}(\times 10^{-15})$ ($A-cm^{-2}$)	ΔJ_{eo} (%)
84.8587	-5.0	178.5	-40.5	357.4	-28.5	108.5	-27.6
85.7519	-4.0	194.8	-35.1	384.0	-23.2	116.9	-22.0
86.6452	-3.0	214.0	-28.7	411.5	-17.7	125.3	-16.5
87.5384	-2.0	237.0	-21.0	439.9	-12.0	133.6	-11.0
88.4317	-1.0	265.1	-11.6	469.4	-6.1	141.8	-5.5
89.3249	0.0	300.0	0.0	500.0	0.0	150.0	0.0
90.2181	1.0	344.7	14.9	531.8	6.4	158.2	5.4
91.1114	2.0	404.1	34.7	565.0	13.0	166.3	10.9
92.0046	3.0	486.7	62.2	599.5	19.9	174.4	16.2
92.8979	4.0	609.6	103.2	635.6	27.1	182.4	21.6
93.7911	5.0	811.6	170.5	673.4	34.7	190.4	26.9

Table 4.15 BSF Model: J_o Fluctuation

Measurement		Solutions					
$J_o(\times 10^{-15})$ ($A-cm^{-2}$)	ΔJ_o (%)	τ_p (μsec)	$\Delta\tau_p$ (%)	S_p ($cm-sec^{-1}$)	ΔS_p (%)	$J_{eo}(\times 10^{-15})$ ($A-cm^{-2}$)	ΔJ_{eo} (%)
370.7365	-5.0	213.0	-29.0	410.2	-18.0	105.4	-29.8
374.6390	-4.0	226.5	-24.5	427.4	-14.5	114.3	-23.8
378.5415	-3.0	241.6	-19.5	445.0	-11.0	123.3	-17.8
382.4440	-2.0	258.5	-13.8	463.0	-7.4	132.2	-11.8
386.3465	-1.0	277.9	-7.4	481.3	-3.7	141.1	-5.9
390.2490	0.0	300.0	0.0	500.0	0.0	150.0	0.0
394.1515	1.0	325.7	8.6	519.1	3.8	158.8	5.9
398.0540	2.0	355.8	18.6	538.7	7.7	167.7	11.8
401.9565	3.0	391.5	30.5	558.6	11.7	176.5	17.6
405.8590	4.0	434.8	44.9	579.1	15.8	185.2	23.5
409.7614	5.0	488.2	62.7	600.0	20.0	194.0	29.3

Table 4.16 BSF Model: W Fluctuation

Measurement		Solutions					
W (μm)	ΔW (%)	τ_p (μsec)	$\Delta\tau_p$ (%)	S_p (cm-sec^{-1})	ΔS_p (%)	$J_{eo}(\times 10^{-15})$ (A-cm^{-2})	ΔJ_{eo} (%)
506.35	-5.0	250.1	-16.6	357.9	-28.4	142.0	-5.3
511.68	-4.0	260.3	-13.2	384.1	-23.2	143.9	-4.1
517.01	-3.0	270.5	-9.8	411.2	-17.8	145.6	-2.9
522.34	-2.0	280.5	-6.5	439.5	-12.1	147.2	-1.9
527.67	-1.0	290.4	-3.2	469.0	-6.2	148.7	-0.9
533.00	0.0	300.0	0.0	500.0	0.0	150.0	0.0
538.33	1.0	309.3	3.1	532.6	6.5	151.2	0.8
543.66	2.0	318.3	6.1	566.9	13.4	152.4	1.6
548.99	3.0	326.9	9.0	603.4	20.7	153.4	2.3
554.32	4.0	335.1	11.7	642.1	28.4	154.3	2.9
559.65	5.0	342.9	14.3	683.5	36.7	155.2	3.5

fluctuations of at least ±5 % in τ_J, τ_V, J_o, and W. Furthermore, for a measurement precision of ±1 %, we can, at best, determine τ_p within 3.1 %, S_p within −3.7 %, and J_{eo} within 0.8 % . At worst, a measurement precision of ±1 % leads to variations in τ_p of 14.9 %, in S_p of 8.4 %, and in J_{eo} of 5.9 %. (Compare these results with those from the Combined Model). Again, observe that the variations increase monotonically with decreasing precision of the experimental data. Moreover, as Tables 4.17 to 4.19 indicate, even if our measurements of τ_J, τ_V, J_o and W are taken with the highest degree of precision, our inability to exactly determine N_D, D_p, and n_i from empirical data can lead to large errors in the solutions for τ_p, S_p, and $J_{éo}$. This is particularly true in the case of n_i. That is, for a measurement precision of ±1% in n_i, variations of −13.6% in τ_p, −7.3% in S_p, and 9.7% in J_{eo} represent the best case scenario.

As a final note, we indicate the crucial importance of exact temperature readings in the BSF Model. We have already discussed in Chapter III the large variation with temperature of the intrinsic carrier concentration, n_i. It is also apparent from Equation 4.21,

$$J_o = J_{sc} \exp\left(-\frac{V_{oc}}{V_T}\right), \tag{4.23}$$

that J_o is highly sensitive to temperature. We shall now study the sensitivities of n_i and J_o to temperature in more detail.

A model for n_i by Barber [14] is written

$$n_i = A T^{1.5} \exp\left(-\frac{0.603}{V_T}\right) \tag{4.24}$$

where T is the absolute temperature, V_T is the thermal voltage, and A is a temperature independent constant equal to 3.10×10^{16}. It is possible to adjust A ($A = 3.516 \times10^{16}$) such that at 25°C, $n_i = 1.20\times10^{10}$ cm^{-3}. This value for n_i is just the baseline value selected for the sensitivity analysis. Referring to Table 4.19, we then calculate the temperature corresponding to the small fluctuations in n_i. We present the results of these temperature calculations in Table 4.20.

In a similar fashion, we can study the temperature dependence of J_o. By appropriate choice of J_{sc} and V_{oc} (J_{sc} = 24.8 mA and V_{oc} = 640 mV) at 25°C, we can set J_o at the baseline value used in the sensitivity analysis. Then, assuming that V_{oc} and J_{sc} are constant with temperature (for the sake of

Table 4.17 BSF Model: N_D Fluctuation

Measurement		Solutions					
$N_D(\times 10^{16})$ (cm^{-3})	ΔN_D (%)	τ_p (μsec)	$\Delta\tau_p$ (%)	S_p ($cm-sec^{-1}$)	ΔS_p (%)	$J_{eo}(\times 10^{-15})$ ($A-cm^{-2}$)	ΔJ_{eo} (%)
1.90	-5.0	213.0	-29.0	410.2	-18.0	110.9	-26.1
1.92	-4.0	226.5	-24.5	427.4	-14.5	119.1	-20.6
1.94	-3.0	241.6	-19.5	445.0	-11.0	127.1	-15.3
1.96	-2.0	258.5	-13.8	463.0	-7.4	134.9	-10.0
1.98	-1.0	277.9	-7.4	481.3	-3.7	142.6	-5.0
2.00	0.0	300.0	0.0	500.0	0.0	150.0	0.0
2.02	1.0	325.7	8.6	519.1	3.8	157.3	4.8
2.04	2.0	355.8	18.6	538.7	7.7	164.4	9.6
2.06	3.0	391.5	30.5	558.6	11.7	171.3	14.2
2.08	4.0	434.8	44.9	579.1	15.8	178.1	18.7
2.10	5.0	488.2	62.7	600.0	20.0	184.8	23.2

Table 4.18 BSF Model: D_p Fluctuation

Measurement		Solutions					
D_p (cm^2–sec^{-1})	ΔD_p (%)	τ_p (μsec)	$\Delta\tau_p$ (%)	S_p (cm–sec^{-1})	ΔS_p (%)	$J_{eo}(\times 10^{-15})$ (A–cm^{-2})	ΔJ_{eo} (%)
9.5	-5.0	410.9	37.0	632.5	26.5	171.3	14.2
9.6	-4.0	383.2	27.7	602.5	20.5	167.1	11.4
9.7	-3.0	358.7	19.6	574.5	14.9	162.8	8.6
9.8	-2.0	337.0	12.3	548.2	9.6	158.6	5.7
9.9	-1.0	317.5	5.8	523.4	4.7	154.3	2.9
10.0	0.0	300.0	0.0	500.0	0.0	150.0	0.0
10.1	1.0	284.2	-5.3	477.8	-4.5	145.7	-2.9
10.2	2.0	269.8	-10.1	456.6	-8.7	141.3	-5.8
10.3	3.0	256.6	-14.5	436.4	-12.7	136.9	-8.7
10.4	4.0	244.6	-18.5	417.1	-16.6	132.5	-11.7
10.5	5.0	233.5	-22.2	398.7	-20.3	128.0	-14.7

Table 4.19 BSF Model: n_i Fluctuation

Measurement		Solutions					
$n_i(\times 10^{10})$ (cm^{-3})	Δn_i (%)	τ_p (μsec)	$\Delta\tau_p$ (%)	S_p ($cm-sec^{-1}$)	ΔS_p (%)	$J_{eo}(\times 10^{-15})$ ($A-cm^{-2}$)	ΔJ_{eo} (%)
1.140	-5.0	1565.2	421.7	732.6	46.5	220.5	47.0
1.152	-4.0	842.5	180.8	677.7	35.5	206.9	37.9
1.164	-3.0	578.0	92.7	627.6	25.5	193.0	28.7
1.176	-2.0	440.8	46.9	581.7	16.3	178.9	19.3
1.188	-1.0	356.8	18.9	539.3	7.9	164.6	9.7
1.200	0.0	300.0	0.0	500.0	0.0	150.0	0.0
1.212	1.0	259.1	-13.6	463.5	-7.3	135.2	-9.9
1.224	2.0	228.2	-23.9	429.5	-14.1	120.1	-20.0
1.236	3.0	204.0	-32.0	397.6	-20.5	104.7	-30.2
1.248	4.0	184.5	-38.5	367.6	-26.5	89.1	-40.6
1.260	5.0	168.6	-43.8	339.5	-32.1	73.2	-51.2

Table 4.20 Temperature Dependence of n_i

$n_i(\times 10^{10}\ cm^{-3})$	$\Delta n_i(\%)$	T(° C)
1.140	-5.0	24.39
1.152	-4.0	24.51
1.164	-3.0	24.63
1.176	-2.0	24.76
1.188	-1.0	24.88
1.200	0.0	25.00
1.212	1.0	25.12
1.224	2.0	25.23
1.236	3.0	25.35
1.248	4.0	25.47
1.260	5.0	25.59

argument), we calculate the temperature necessary to cause the small fluctuations in J_o in Table 4.15. We present the results of the temperature sensitivities of J_o in Table 4.21.

The results, besides demonstrating the close relationship between n_i and J_o (compare the third column of Tables 4.20 and 4.21), demonstrate that the ± 1 % fluctuation in the experimental measurement of n_i and J_o can be caused by an error of only $\pm 0.12^\circ$ C in temperature. Also, we have assumed that our models for n_i and J_o are known exactly. The model for n_i, however, is empirical and is reported with ± 5 % accuracy at room temperature [14]. Similarly, the model for J_o assumes that the junction perfection factor, n, is equal to one. However, discrepancies in n of only 1 %, as seen in Equation 4.23, correspond to a temperature fluctuation of $\sim 300^\circ$ C $\times$ 1 % = 3° C.

4.5 Study of the Integrated Recombination

One explanation for the large variations in the values of the solution variables, τ_p, S_p, and J_{eo}, may be that the cell recombination itself is largely insensitive to these solution values. We check this hypothesis by performing a study of the integrated recombination in the solar cell using the solar cell analysis program, SCAP1D [17]. The study allows us to examine the distribution of the total recombination into emitter, base, and back surface components. The results of the study indicate that, contrary to our hypothesis, the distribution of the total recombination is indeed sensitive to the values for τ_p, S_p, and J_{eo}. Hence, small uncertainties in the experimental measurements and the empirical data can lead to radically different interpretations of the recombination in the BSF solar cell using the Combined and BSF Models.

In the following section, we elaborate on the hypothesis originally introduced to explain the insensitivities associated with the Combined Model and the BSF Model. We then test this hypothesis by a study of the integrated recombination using SCAP1D. We conclude by presenting results which disprove the hypothesis and by discussing the implications of these findings.

4.5.1 Hypothesis

In Section 4.4, we observed large variations in the solutions of the Combined Model and the BSF Model to small perturbations in the experimental measurements. The largest variations, we recall, occurred for τ_p (and τ_{p_r}), S_p, and J_{eo}. Since the cells have values of τ_p, S_p, and J_{eo} typical of

Table 4.21 Temperature Dependence of J_o

$J_o(\times 10^{-15}$ A–cm$^{-2})$	$\Delta J_o(\%)$	T(° C)
370.7365	-5.0	24.39
374.6390	-4.0	24.51
378.5415	-3.0	24.64
382.4440	-2.0	24.76
386.3465	-1.0	24.88
390.2490	0.0	25.00
394.1515	1.0	25.12
398.0540	2.0	25.24
401.9565	3.0	25.36
405.8590	4.0	25.47
409.7614	5.0	25.59

high quality solar cells, it may be that even large variations in these parameters have little effect on the distribution of the total recombination in the cell. For example, a high base lifetime such as $\tau_p = 300 \times 10^{-6}$ sec indicates very little recombination in the base. As long as the lifetime is high, that is, much greater than the lifetimes usually associated with lossy bases (1 μ sec, for example) the exact value of the lifetime may be unimportant. Much the same can be said for the back surface recombination velocity. In BSF solar cells, S_p is quite low. As long as S_p is much less than the values at which the back surface becomes lossy (10^4 cm–sec^{-1}, for example) the exact value of this parameter may be of little significance. Similar statements may also be applicable for J_{eo}. That the distribution of the total recombination is insensitive to precise values for τ_p, S_p, and J_{eo} may explain then the large variations in τ_p, S_p, and J_{eo} that we encounter for small uncertainties in the experimental measurements.

4.5.2 Test of the Hypothesis

To test the hypothesis made in the preceding section, we study the integrated minority carrier recombination in the solar cell using the solar cell analysis program, SCAP1D. Our objective is to find the variation in the distribution of the total recombination for the emitter, base, and back surface components, corresponding to the variations in τ_p, S_p, and J_{eo} found during the sensitivity analysis of the BSF Model in Section 4.4.2.

In the following sections, we briefly describe the utility of SCAP1D in determining the distribution of recombination in the solar cell and the procedures used to study the redistribution of the recombination for variations in τ_p, S_p, and J_{eo}.

4.5.2.1 Utility of SCAP1D

SCAP1D, a numerical model of the solar cell developed at Purdue University, provides numerous details of the solar cell behavior for a variety of input conditions. In fact, for an illuminated cell under open circuit voltage conditions it is possible to determine the distribution of the total cell recombination into emitter, base, and back surface components. This is possible since, under open circuit voltage conditions, all minority carriers generated in the cell recombine and the recombination rate, described by the SCAP1D model equations, can be computed throughout the entire cell. From

plots generated by SCAP1D in which the recombination rate is integrated through the full width of the cell, we can thus determine the amount of recombination which is attributable to the emitter, base, and back surface regions.

4.5.2.2 Test Procedure

We begin by setting τ_p and S_p at the baseline values selected in the sensitivity analysis for the BSF Model. That is, $\tau_p = 300\ \mu$sec and $S_p = 500$ cm–sec^{-1}. We then adjust the emitter lifetime in SCAP1D in order to set J_{eo} equal to its baseline value in the sensitivity analysis, $J_{eo} = 150 \times 10^{-15}$ amps–cm^{-2}. Also, for consistency, the cell width is selected to be 533 microns and the base doping, 2×10^{16} cm^{-3}. The intrinsic carrier concentration and the diffusion coefficient in the base, however, are determined directly from models in SCAP1D. For the temperature selected (T = 28° C), $n_i = 1.3464 \times 10^{10}$ cm^{-3} and $D_p = 11.0$ cm-sec^{-1}. Although these values do not match exactly those assumed in the sensitivity analysis ($n_i = 1.20 \times 10^{10}$ cm^{-3} and $D_p = 10.0$ cm-sec^{-1}), the qualitative nature of our results, we shall see, is not affected. With these parameters, we now make a run of SCAP1D under AM1.0 conditions. From the plots of the integrated recombination under open circuit voltage conditions, we determine the distribution, in percent, of the total recombination into emitter, base, and back surface components. We record these findings in Table 4.22. Note that for the parameters assumed for the cell, the recombination is fairly evenly distributed into emitter, base, and back surface components.

From the cell information given above we can calculate from the BSF Model equations the "measurements" necessary to render the assumed solutions for τ_p, S_p, and J_{eo}. In the same manner as that used for the sensitivity analysis of the BSF Model in Section 4.4.2, we can use our program to construct tables of the variation of τ_p, S_p, and J_{eo} to small fluctuations in the experimental measurements. We do this for a more limited set of fluctuations (just ± 1, ± 2, and ± 5 %) and record the results in Tables 4.23 to 4.29. Note that these tables correspond closely with those in the original sensitivity analysis (Tables 4.13 through 4.19). Exact correspondence is not possible because of the slightly different values for n_i and D_p. However, as noted earlier, the qualitative nature of the results is unaffected.

We now use the set of values for τ_p, S_p, and J_{eo} determined from each fluctuation to calculate the redistribution of the total recombination. We

Table 4.22 Distribution of Total Recombination: Baseline Cell

Location	Recombination Parameter	Percent Composition of Total Recombination
Base	$\tau_p = 300\ \mu$sec	30.9
Back Surface	$S_p = 500$ cm-sec^{-1}	37.7
Emitter	$J_{eo} = 150 \times 10^{-15}$ A-cm^{-2}	31.4

Table 4.23 Distribution of Total Recombination : τ_J Fluctuation

Measurement		Solutions								
		Base			Back Surface			Emitter		
τ_J (μsec)	$\Delta\tau_J$ (%)	τ_p (μsec)	$\Delta\tau_p$ (%)	Comp. (%)	S_p (cm−sec^{-1})	ΔS_p (%)	Comp. (%)	$J_{eo}(\times10^{-15})$ (A−cm^{-2})	ΔJ_{eo} (%)	Comp. (%)
37.9399	-5.0	613.5	104.5	15.2	739.1	47.8	46.5	184.4	23.0	38.3
-	-	-	-	-	-	-	-	-	-	-
-	-	-	-	-	-	-	-	-	-	-
39.5373	-2.0	376.07	25.4	24.5	583.7	16.7	41.4	163.6	9.1	34.1
39.5373	-1.0	333.6	11.2	28.0	540.2	8.0	39.3	156.8	4.5	32.7
39.3361	0.0	300.0	0.0	30.9	500.0	0.0	37.7	150.0	0.0	31.4
40.3361	1.0	272.7	-9.1	34.1	462.7	-7.5	36.0	143.3	-4.5	29.9
40.7354	2.0	250.0	-16.7	37.1	427.9	-14.4	34.4	136.6	-8.9	28.5
-	-	-	-	-	-	-	-	-	-	-
-	-	-	-	-	-	-	-	-	-	-
41.9335	5.0	200.4	-33.2	46.0	336.3	-32.7	29.2	116.8	-22.1	24.8

Table 4.24 Distribution of Total Recombination: τ_V Fluctuation

Measurement		Solutions								
		Base			Back Surface			Emitter		
τ_V (μsec)	$\Delta\tau_V$ (%)	τ_p (μsec)	$\Delta\tau_p$ (%)	Comp. (%)	S_p (cm−sec^{-1})	ΔS_p (%)	Comp. (%)	$J_{eo}(\times 10^{-15})$ (A−cm^{-2})	ΔJ_{eo} (%)	Comp. (%)
87.5070	-5.0	176.0	-41.3	51.2	362.0	-27.6	29.0	94.8	-36.8	19.8
-	-	-	-	-	-	-	-	-	-	-
-	-	-	-	-	-	-	-	-	-	-
90.2703	-2.0	235.3	-21.6	39.1	442.2	-11.6	34.1	128.1	-14.6	19.8
91.1915	-1.0	264.0	-12.0	34.9	470.6	-5.9	36.1	139.1	-7.2	29.0
92.1126	0.0	300.0	0.0	30.9	500.0	0.0	37.7	150.0	0.0	31.4
93.0337	1.0	346.6	15.5	27.0	530.4	6.1	39.4	160.9	7.2	33.6
93.9549	2.0	409.3	36.4	23.0	561.8	12.4	41.2	171.7	14.4	42.2
-	-	-	-	-	-	-	-	-	-	-
-	-	-	-	-	-	-	-	-	-	-
96.7182	5.0	866.8	188.9	11.3	663.4	32.7	46.5	203.8	35.9	42.2

Table 4.25 Distribution of Total Recombination: J_o Fluctuation

Measurement		Solutions								
		Base			Back Surface			Emitter		
$J_o(\times 10^{-15})$ (A-cm^{-2})	ΔJ_o (%)	τ_p (μsec)	$\Delta\tau_p$ (%)	Comp. (%)	S_p (cm-sec^{-1})	ΔS_p (%)	Comp. (%)	$J_{eo}(\times 10^{-15})$ (A-cm^{-2})	ΔJ_{eo} (%)	Comp. (%)
445.88	-5.0	207.0	-31.0	46.0	408.3	-18.3	33.8	91.0	-39.3	20.2
-	-	-	-	-	-	-	-	-	-	-
-	-	-	-	-	-	-	-	-	-	-
459.97	-2.0	255.0	-15.0	36.8	462.3	-7.5	36.2	126.5	-15.7	27.0
464.66	-1.0	275.8	-8.1	34.1	481.0	-3.8	36.9	138.3	-7.8	29.0
469.35	0.0	300.0	0.0	30.9	500.0	0.0	37.7	150.0	0.0	31.4
474.04	1.0	328.5	9.5	28.0	519.4	3.9	38.6	161.7	7.8	33.4
478.74	2.0	362.5	20.8	25.2	539.2	7.8	39.3	173.3	15.6	35.5
-	-	-	-	-	-	-	-	-	-	-
-	-	-	-	-	-	-	-	-	-	-
492.82	5.0	521.0	73.7	17.3	601.1	20.2	41.6	208.1	38.7	41.1

Table 4.26 Distribution of Total Recombination: W Fluctuation

Measurement		Solutions								
		Base			Back Surface			Emitter		
W (μm)	ΔW (%)	τ_p (μsec)	$\Delta\tau_p$ (%)	Comp. (%)	S_p (cm–sec^{-1})	ΔS_p (%)	Comp. (%)	$J_{eo}(\times 10^{-15})$ (A–cm^{-2})	ΔJ_{eo} (%)	Comp. (%)
506.35	-5.0	243.1	-19.0	38.3	355.5	-28.9	32.7	138.2	-7.9	29.0
-	-	-	-	-	-	-	-	-	-	-
-	-	-	-	-	-	-	-	-	-	-
522.34	-2.0	277.4	-7.5	33.4	438.9	-12.2	36.2	145.8	-2.8	30.4
527.67	-1.0	288.7	-3.8	32.1	468.8	-6.2	36.9	148.0	-1.3	31.0
533.00	0.0	300.0	0.0	30.9	500.0	0.0	37.7	150.0	0.0	31.4
538.33	1.0	311.1	3.7	29.8	532.6	6.5	38.5	151.8	1.2	31.7
543.66	2.0	321.9	7.3	28.6	566.9	13.4	39.3	153.5	2.4	32.1
-	-	-	-	-	-	-	-	-	-	-
-	-	-	-	-	-	-	-	-	-	-
559.65	5.0	352.6	17.5	26.2	681.8	36.4	41.1	157.8	5.2	32.7

Table 4.27 Distribution of Total Recombination: n_i Fluctuation

Measurement		Solutions								
		Base			Back Surface			Emitter		
$n_i(\times 10^{10})$ (cm^{-3})	Δn_i (%)	τ_p (μsec)	$\Delta\tau_p$ (%)	Comp. (%)	S_p ($cm-sec^{-1}$)	ΔS_p (%)	Comp. (%)	$J_{eo}(\times 10^{-15})$ ($A-cm^{-2}$)	ΔJ_{eo} (%)	Comp. (%)
1.279	-5.0	2702.7	800.9	3.3	733.6	46.7	45.7	247.7	65.2	51.0
-	-	-	-	-	-	-	-	-	-	-
-	-	-	-	-	-	-	-	-	-	-
1.319	-2.0	462.6	54.2	19.8	582.6	16.5	40.8	190.1	26.7	39.4
1.333	-1.0	363.7	21.2	26.1	539.8	8.0	39.1	170.2	13.5	34.8
1.346	0.0	300.0	0.0	30.9	500.0	0.0	37.7	150.0	0.0	31.4
1.360	1.0	255.6	-14.8	36.6	462.8	-7.4	36.1	129.4	-13.7	27.3
1.373	2.0	222.8	-25.7	42.9	428.1	-14.4	34.4	108.5	-27.7	22.7
-	-	-	-	-	-	-	-	-	-	-
-	-	-	-	-	-	-	-	-	-	-
1.414	5.0	161.4	-46.2	60.9	335.6	-32.9	29.8	43.5	-71.0	9.3

Table 4.28 Distribution of Total Recombination: N_D Fluctuation

Measurement		Solutions								
		Base			Back Surface			Emitter		
$N_D(\times 10^{16})$ (cm^{-3})	ΔN_D (%)	τ_p (μsec)	$\Delta\tau_p$ (%)	Comp. (%)	S_p ($cm-sec^{-1}$)	ΔS_p (%)	Comp. (%)	$J_{eo}(\times 10^{-15})$ ($A-cm^{-2}$)	ΔJ_{eo} (%)	Comp. (%)
1.90	-5.0	207.0	-31.0	44.7	408.3	-18.3	33.9	95.8	-36.1	21.4
-	-	-	-	-	-	-	-	-	-	-
-	-	-	-	-	-	-	-	-	-	-
1.96	-2.0	255.0	-15.0	36.4	462.3	-7.5	36.5	129.1	-13.9	27.1
1.98	-1.0	275.8	-8.1	33.9	481.0	-3.8	37.1	139.7	-6.9	29.0
2.00	0.0	300.0	0.0	30.9	500.0	0.0	37.7	150.0	0.0	31.4
2.02	1.0	328.5	9.5	28.6	519.4	3.9	38.3	160.1	6.7	33.1
2.04	2.0	362.5	20.8	25.5	539.2	7.8	39.1	169.9	13.3	35.4
-	-	-	-	-	-	-	-	-	-	-
-	-	-	-	-	-	-	-	-	-	-
2.10	5.0	521.0	73.7	17.9	601.1	20.2	41.0	198.2	32.1	41.1

Table 4.29 Distribution of Total Recombination: D_p Fluctuation

Measurement		Solutions								
		Base			Back Surface			Emitter		
D_p (cm^2–sec^{-1})	ΔD_p (%)	τ_p (μsec)	$\Delta\tau_p$ (%)	Comp. (%)	S_p (cm–sec^{-1})	ΔS_p (%)	Comp. (%)	$J_{eo}(\times 10^{-15})$ (A–cm^{-2})	ΔJ_{eo} (%)	Comp. (%)
10.45	-5.0	430.5	43.5	21.3	632.3	26.5	41.3	179.8	19.9	37.4
-	-	-	-	-	-	-	-	-	-	-
-	-	-	-	-	-	-	-	-	-	-
10.78	-2.0	342.2	14.1	26.8	548.5	9.7	39.3	162.0	8.0	33.9
10.98	-1.0	319.8	6.6	29.1	523.6	4.7	38.6	156.0	4.0	32.3
11.00	0.0	300.0	0.0	30.9	500.0	0.0	37.7	150.0	0.0	31.4
11.11	1.0	282.3	-5.9	32.8	477.5	-4.5	37.1	143.9	-4.1	30.1
11.22	2.0	266.5	-11.2	35.0	456.0	-8.8	36.3	137.8	-8.1	28.7
-	-	-	-	-	-	-	-	-	-	-
-	-	-	-	-	-	-	-	-	-	-
11.55	5.0	227.3	-24.2	41.0	396.7	-20.7	33.6	119.2	-20.6	25.4

simply set τ_p and S_p in SCAP1D to their new values caused by the fluctuation in the experimental measurement under study. Since the base component of the dark current changes somewhat for the new values of τ_p and S_p, it is necessary to again adjust the emitter lifetime in SCAP1D so that the measurement of the total saturation current, J_o, is satisfied. The new distribution of the recombination into emitter, base, and back surface components is then recorded in Tables 4.23 to 4.29 under the heading "Comp." (percent composition) for comparison with τ_p, S_p, and J_{eo}.

4.5.3 Discussion of the Results

In Tables 4.23 to 4.29, we observe that a small fluctuation in the experimental measurements leads not only to large variations in τ_p, S_p, and J_{eo}, but also to large variations in the distribution of the total recombination into emitter, base, and back surface components. Variations, in fact, can be so large that radically different interpretations of device behavior can result. For example, the -5 % fluctuation in n_i indicates negligible base recombination, while the $+5$ % fluctuation indicates negligible emitter recombination. While fluctuations in the other parameters have a less severe effect, the correct interpretation of device behavior remains a problem. For example, the -5 % fluctuation in τ_J indicates a low loss base and a high loss back surface, while the $+5$ % fluctuation indicates just the opposite. Again, remember that we have not included the more likely possibility of fluctuations in all the measurements at once.

As a final note, we observe that, throughout the range of fluctuation made for each experimental measurement, the solar cell performance parameters (that is, the open circuit voltage, V_{oc}, the short circuit current, J_{sc}, the fill factor, FF, and the efficiency, η) computed by SCAP1D are essentially unchanged. Hence, devices with radically different internal behavior can exhibit the same external behavior. The Rose-Weaver Method, therefore, unless done with extremely tight precision, is not able to distinguish among a set of devices with similar external behavior, the internal mechanisms which limit the performance of each particular device.

In summary, we prove false our hypothesis that, for the high quality BSF solar cells under consideration, exact values of τ_p, S_p, and J_{eo} are unimportant. Instead, it is apparent that extreme care must be taken to reduce the uncertainty in the experimental measurements and the empirical parameters when using the BSF Model to determine τ_p, S_p, and J_{eo}. As we have seen,

accurate knowledge of τ_p, S_p, and J_{eo} is necessary if we wish to properly determine the distribution of the total cell recombination into emitter, base, and back surface components. Only then will we be able to identify where to focus our efforts in the design of an optimal efficiency solar cell.

CHAPTER V
SUMMARY AND RECOMMENDATIONS

5.1 Summary

While the Combined Model, in theory, is highly desirable because of its independence of empirical parameters, extremely precise measurements of the short circuit current and open circuit voltage decay rates and of the total saturation current density are required for its implementation. Typical uncertainties presently encountered in the laboratory for these measurements indicate the use of the Combined Model to be highly unreliable. In order for the Combined Model to be useful, significant improvement in measurement precision is required.

Use of the BSF Model, while allowing greater uncertainty in the experimental measurements, is complicated by the need to precisely know the empirical parameters n_i, D_p, and N_D.

5.2 Recommendations

In all likelihood an extremely accurate model for n_i does not seem feasible. It would be best to eliminate n_i entirely from the model equations. Hence, we should focus our efforts on the Combined Model, which is independent of empirical parameters, rather than on the BSF Model.

Further improvement, however, is necessary for the Combined Model. First, we must maintain constant temperature between the back surface field and back surface field removal experiments. This condition is necessary for the simultaneity of the Combined Model equations. Secondly, we must perfect the back surface field removal technique such that the base lifetime is not impaired. In this manner, we will be able to reduce the number of unknowns in the system of equations and enhance system simplicity. Finally, we must be aware of the occurrence of singularities in the model equations. Removal of those equations containing singularities is likely to improve the system sensitivity.

LIST OF REFERENCES

LIST OF REFERENCES

[1] R. J. Schwartz and J. L. Gray, "Two-Dimensional Computer Simulation of Single Crystal Silicon Concentrator Cells," *Proceedings of the Seventeenth IEEE Photovoltaic Specialists Conference,* pp. 1297-1302, May 1-4, 1984.

[2] R. J. Schwartz and J. L. Gray, "Performance Limits of Silicon Solar Cells," *Solar Cells,* vol. 12, pp. 197-203, 1984.

[3] B. H. Rose and H. T. Weaver, "Determination of Effective Surface Recombination Velocity and Minority Carrier Lifetime in High-Efficiency Silicon Solar Cells," *Journal of Applied Physics,* vol. 54, pp. 238-247, 1983.

[4] H. J. Hovel, *Solar Cells (Semiconductors and Semimetals Series, vol. 11),* Academic Press, New York, N. Y., 1975.

[5] S. M. Sze, *Physics of Semiconductor Devices,* John Wiley and Sons, New York, N. Y., 1981.

[6] Edward S. Yang, *Fundamentals of Semiconductor Devices,* McGraw-Hill, New York, N. Y., p. 99, 1978.

[7] G. V. Ram and M. S. Tyagi, "Effective Recombination Velocity at the NN^+ Interface," *Solid-State Electronics,* vol. 24, no. 8, pp. 753-761, 1981.

[8] I. S. Sokolnikoff and R. M. Redheffer, *Mathematics of Physics and Modern Engineering,* McGraw-Hill, New York, N. Y., pp. 467-470, 1966.

[9] A. R. Moore, "Carrier Lifetime in Photovoltaic Solar Cells by the Small-Signal Open-Circuit Decay Method," *RCA Review,* vol. 41, pp. 549-562, Dec. 1980.

[10] Jerry G. Fossum, Frederick Lindholm, and M. Ayman Shibib, "The Importance of Surface Recombination and Energy Band Gap Narrowing in P-N Junction Solar Cells," *IEEE Transactions on Electron Devices,* vol. ED-26, no. 9, pp. 1294-1298, 1979.

[11] B. H. Rose and H. T. Weaver, "Emitter Recombination and Minority Carrier Lifetime Measurements on High-Efficiency Silicon Solar Cells," *Proceedings of the Seventeenth IEEE Photovoltaics Specialists Conference,* pp. 626-631, May 1-4, 1984.

[12] S. C. Jain and U. C. Ray, "Photovoltage Decay in P-N Junction Solar Cells Including the Effects of Recombinations in the Emitter," *Journal of Applied Physics,* vol. 54, pp. 2079-2085, 1983.

[13] Roy A. Colclaser, *Microelectronics: Processing and Device Design,* John Wiley and Sons, New York, N. Y., 1980.

[14] H. D. Barber, "Effective Mass and Intrinsic Concentration in Silicon," *Solid-State Electronics,* vol. 10, pp. 1039-1051, 1967.

[15] Jacob Millman, *Micro-electronics: Digital and Analog Circuits and Systems,* McGraw-Hill, New York, N. Y., 1979.

[16] T. J. Aird, "SECANT," Purdue University Computing Center Subroutine Library, 1970.

[17] M. S. Lundstrom, "Numerical Analysis of Silicon Solar Cells," Ph.D Thesis, Purdue University, 1980.

[18] Philip Wolfe, "The Secant Method for Simultaneous Nonlinear Equations," *Communications of the ACM,* vol. 2, pp. 12-13, 1959.

[19] A. P. French and Edwin F. Taylor, *An Introduction to Quantum Physics,* W. W. Norton and Co., Inc., New York, N. Y., p. 160, 1978.

APPENDICES

Appendix A: Demonstration of First Order Decay Term Dominance

For the short circuit current decay rate, the appropriate expression is

$$\frac{1}{\tau_{J_m}} = \beta_{J_m}^2 D_p + \frac{1}{\tau_p} \tag{2.21}$$

where

$$\beta_{J_m} \cot \beta_{J_m} W = -\frac{S_p}{D_p} . \tag{2.20}$$

Solutions of Equation 2.20 for the short circuit current decay eigenvalue, β_{J_m}, can be found graphically [19], as shown in Figure A1.

From the graph we observe that, as the index m increases, β_{J_m} becomes larger and causes τ_{J_m} in Equation 2.21 to progressively decrease. D_p, W, τ_p, and S_p are, of course, fixed in value.

A similar analysis applies in the case of the open circuit voltage decay. Here, the corresponding decay rate equation is

$$\frac{1}{\tau_{V_m}} = \beta_{V_m}^2 D_p + \frac{1}{\tau_p} \tag{2.26}$$

where

$$\beta_{V_m} \tan \beta_{V_m} W = \frac{S_p}{D_p} . \tag{2.25}$$

Solutions of Equation 2.25 for the open circuit voltage decay eigenvalue, β_{J_m}, can again be found graphically, as shown in Figure A2.

Thus, as the index m increases, β_{V_m} becomes larger and causes τ_{V_m} in Equation 2.26 to progressively decrease.

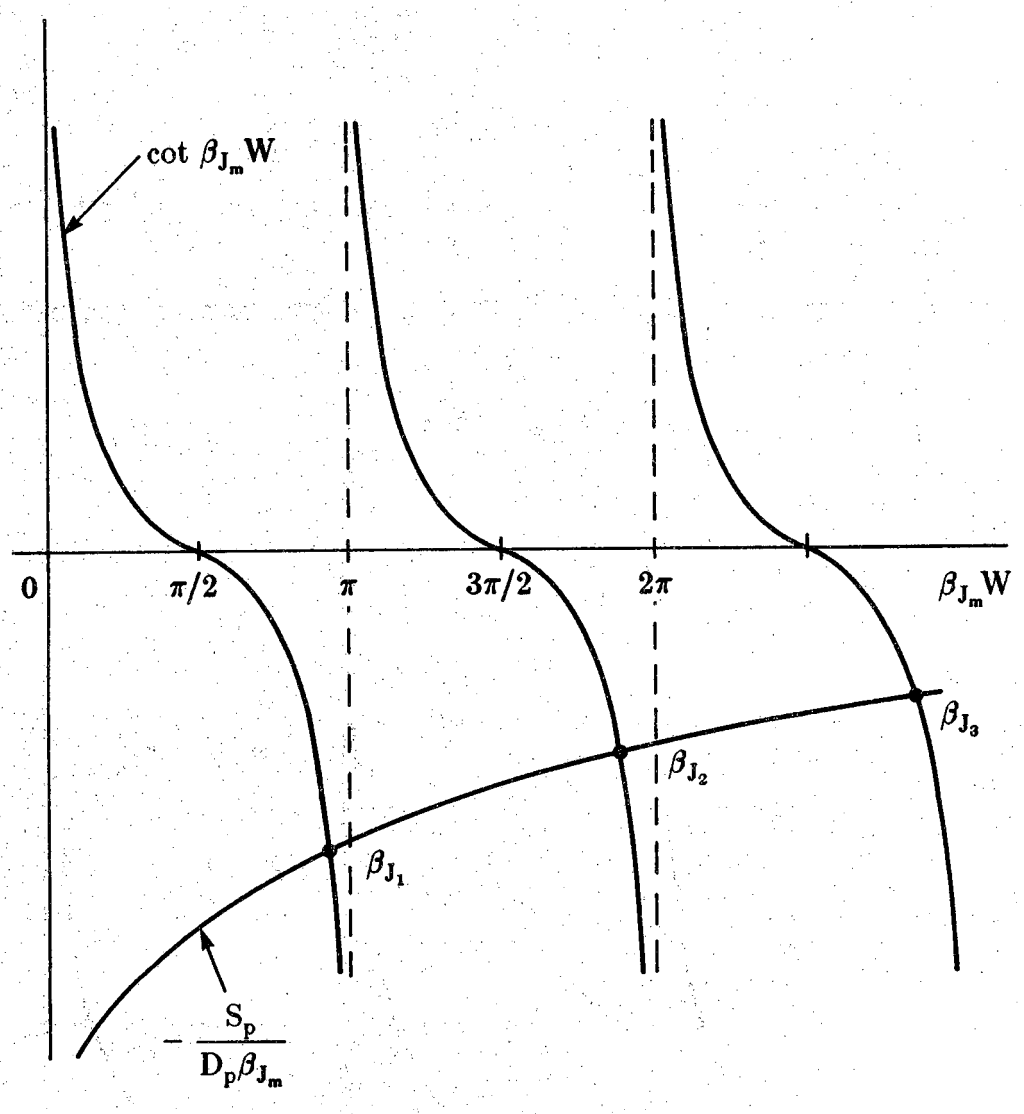

Figure A1 Graphical Solution of β_{J_m}.

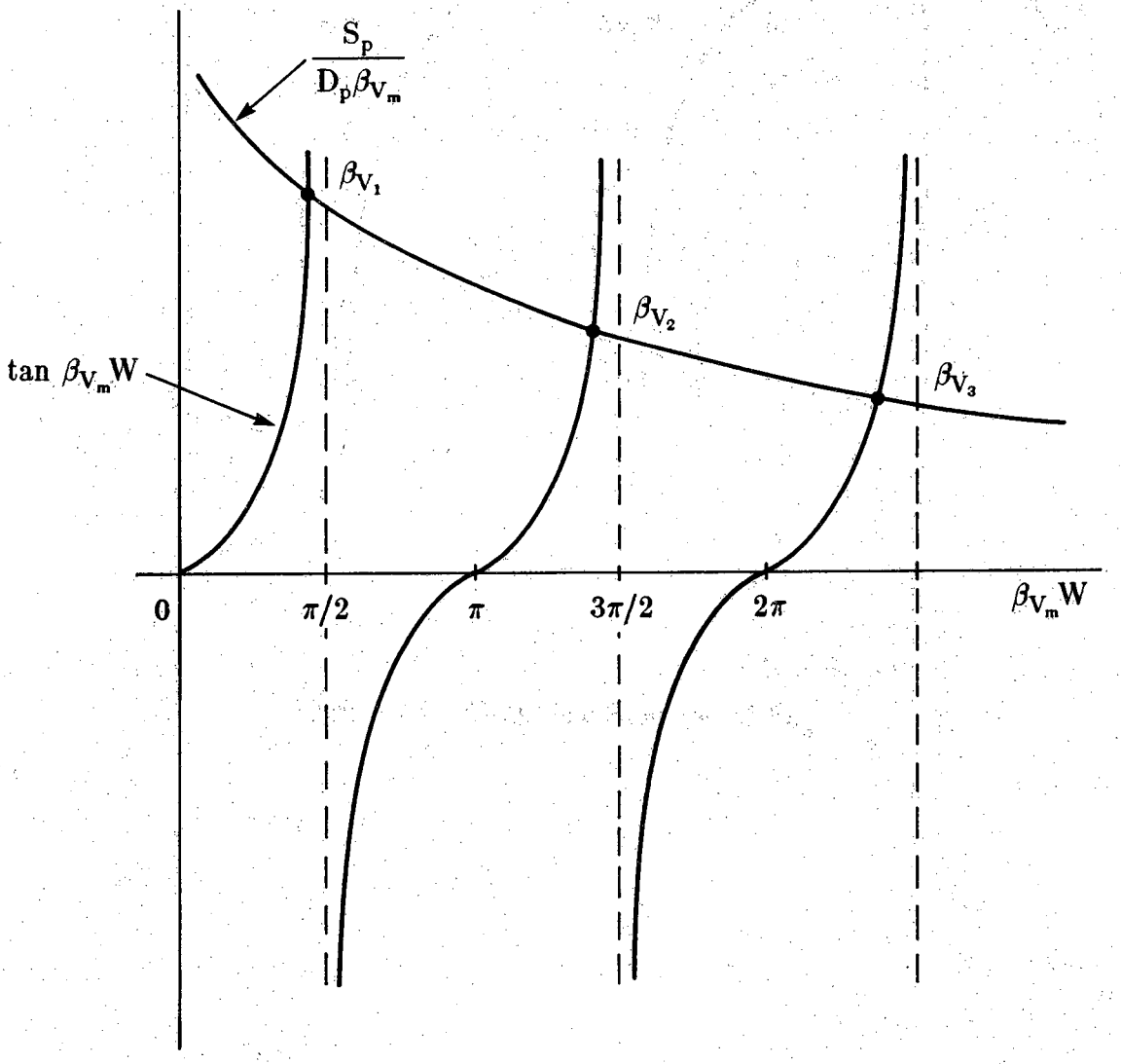

Figure A2 Graphical Solution of β_{V_m}.

Appendix B: Small-Signal Approximation for the Open Circuit Voltage Decay

For the open circuit voltage subject to a light bias and a small-signal perturbation, we have (Equation 2.34)

$$V_{oc}(t) = n V_T \ln\left[\frac{\Delta p_{n_B} + \Delta p_{n_V}(x,t)}{p_{no}} + 1\right]\Bigg|_{x=0}.$$

Assuming $\left(\Delta p_{n_B} + \Delta p_{n_V}(x,t)\right)/p_{no} >> 1$, then

$$V_{oc}(t) = n V_T \ln\left[\frac{\Delta p_{n_B} + \Delta p_{n_V}(x,t)}{p_{no}}\right]\Bigg|_{x=0}$$

$$= n V_T \ln\left[\frac{\Delta p_{n_B}}{p_{no}}\left(1 + \frac{\Delta p_{n_V}(x,t)}{\Delta p_{n_B}}\right)\right]_{x=0}$$

$$= n V_T \left[\ln\frac{\Delta p_{n_B}}{p_{no}} + \ln\left(1 + \frac{\Delta p_{n_V}(x,t)}{\Delta p_{n_B}}\right)\right]_{x=0}.$$

Making the small-signal approximation $\Delta p_{n_V}(x,t) << \Delta p_{n_B}$ [9], it is then true that

$$\ln\left[1 + \frac{\Delta p_{n_V}(x,t)}{\Delta p_{n_B}}\right] \simeq \frac{\Delta p_{n_V}(x,t)}{\Delta p_{n_B}}$$

Thus,

$$V_{oc}(t) = n V_T \left[\ln \frac{\Delta p_{n_B}}{p_{no}} + \frac{\Delta p_{n_V}(x,t)}{\Delta p_{n_B}} \right] \Bigg|_{x=0}$$

$$= n V_T \ln \frac{\Delta p_{n_B}}{p_{no}} + n V_T \frac{\Delta p_{n_V}(x,t)}{\Delta p_{n_B}} \Bigg|_{x=0}.$$

Substituting for $\Delta p_{n_V}(x,t)$ from Equation 2.24,

$$V_{oc}(t) = n V_T \ln \frac{\Delta p_{n_B}}{p_{no}} + \frac{n V_T}{\Delta p_{n_B}} \sum_{m=1}^{\infty} C_{V_m} \exp\left[-\frac{t}{\tau_{V_m}} \right].$$

Renaming constants, we derive the expression for the open circuit voltage given in Equation 2.35:

$$V_{oc}(t) = V_B + \sum_{m=1}^{\infty} V_{oc_m} \exp\left[-\frac{t}{\tau_{V_m}} \right]$$

where

$$V_B = n V_T \ln \left[\frac{\Delta p_{n_B}}{p_{no}} \right],$$

$$V_{oc_m} = \frac{n V_T}{\Delta p_{n_B}} C_{V_m},$$

and

$$\frac{1}{\tau_{V_m}} = \beta_{V_m}^2 D_p + \frac{1}{\tau_p}.$$

Appendix C: SECANT

SECANT, an algorithm for the simultaneous solution of a system of non-linear equations, is based on a generalization of the secant method for a single function of one variable [18]. In order to adapt SECANT for use in our program, we first treat three numerical problems in the system of Combined Model equations. These problems are singularities, square roots, and scaling. After taking care of these problems, we convert the system of equations to Fortran in preparation for its solution by SECANT. Next, we describe the procedure for calling SECANT in the program. An important step of this procedure is to provide SECANT with a suitable initial guess to the solution. We include, at the end of this appendix, a listing of our Fortran program featuring SECANT.

C.1 Numerical Problems

C.1.1 Singularities

At times, the argument, $\beta_V W$, of the tangent function in Equation 4.12 must pass through the singularity at $\pi/2$ in order to reach a solution. This occurs because solutions for $\beta_V W$ exist for radian angles between 0 and π. Near the singularity the value of the tangent function becomes impractically large and the solution procedure stalls. The problem of the singularity can be solved rather simply by placing the tangent function in the denominator. In this way, when it is necessary for the argument of the tangent function to pass through $\pi/2$, the function will be well-behaved and pose no threat to the solution process.

No special precautions need be taken for the cotangent function in the system. Physical solutions of the argument for the cotangent lie entirely between $\pi/2$ and π. The cotangent function thus never passes through its singularity at π.

C.1.2 Square Roots

SECANT has difficulty solving equations containing square roots. Apparently, during the solution process, the argument of the square root can pass through negative values, causing the program to fail. The square roots can be removed from the equations using the definition of the diffusion length, $L = \sqrt{D\tau}$. By means of the diffusion length, we will in fact remove the minority carrier lifetimes, τ_p, and τ_{p_r}, entirely from the system. Thus, L_p and L_{p_r} now become the independent solution variables in the system. τ_p and τ_{p_r} are then dependent variables, calculated from the diffusion length definition.

Incorporating the modifications due to singularities and square roots, our set of eight simultaneous equations takes on the following form:

$$\beta_J \cot \beta_J W = -\frac{S_p}{D_p} \tag{C.1}$$

$$\beta_V + \frac{S_p \beta_{V_r} \cot \beta_{V_r} W_r}{D_p \beta_V} = \frac{1}{\tan \beta_V W}\left[\frac{S_p}{D_p} - \beta_{V_r} \cot \beta_{V_r} W_r\right] \tag{C.2}$$

$$\frac{1}{\tau_J} = \beta_J^2 D_p + \frac{D_p}{L_p^2} \tag{C.3}$$

$$\frac{1}{\tau_V} = \beta_V^2 D_p + \frac{D_p}{L_p^2} \tag{C.4}$$

$$J_o = -q\, p_{no} D_p \beta_{V_r} \cot \beta_{V_r} W_r + q\, p_{no} \frac{D_p}{L_p}\left[\frac{\frac{S_p L_p}{D_p} + \tanh \frac{W}{L_p}}{1 + \frac{S_p L_p}{D_p} \tanh \frac{W}{L_p}}\right] \tag{C.5}$$

$$\frac{1}{\tau_{J_r}} = \left(\frac{\pi}{W_r}\right)^2 D_p + \frac{D_p}{L_{p_r}^2} \tag{C.6}$$

$$\frac{1}{\tau_{V_r}} = \beta_{V_r}^2 D_p + \frac{D_p}{L_{p_r}^2} \tag{C.7}$$

$$J_{o_r} = -q\, p_{no} D_p \beta_{V_r} \cot \beta_{V_r} W_r + q\, p_{no} \frac{D_p}{L_{p_r}} \coth \frac{W_r}{L_{p_r}} . \tag{C.8}$$

The eight independent solution variables in the system are β_J, β_V, D_p, S_p, L_p, p_{no}, β_{V_r}, and L_{p_r}; while J_{eo}, τ_p, and τ_{p_r} are dependent solution variables whose values can be found from the following relations:

$$J_{eo} = -q\, p_{no} D_p \beta_{V_r} \cot \beta_{V_r} W_r \tag{C.9}$$

$$\tau_p = \frac{L_p^2}{D_p} \tag{C.10}$$

$$\tau_{p_r} = \frac{L_{p_r}^2}{D_p} . \tag{C.11}$$

C.1.3 Scaling

SECANT requires that the solution variables have values of roughly comparable magnitude. An examination of a typical solution for the system of equations illustrates quite clearly the need for scaling.

$$S_p = 300 \ \text{cm–sec}^{-1}$$

$$p_{no} = 1.0 \times 10^4 \ \text{cm}^{-3}$$

$$D_p = 10 \ \text{cm}^2\text{–sec}^{-1}$$

$$\beta_J = 50 \ \text{cm}^{-1}$$

$$\beta_V = 30 \ \text{cm}^{-1}$$

$$\beta_{V_r} = 30 \ \text{cm}^{-1}$$

$$L_p = 5.0 \times 10^{-2} \ \text{cm}$$

$$L_{p_r} = 5.0 \times 10^{-2} \ \text{cm}$$

In this set, the values for the solution variables range over approximately six orders of magnitude, making a numerical solution difficult as some variables will have little weight compared to the others. By introducing scaling factors, we can overcome the above discrepancy and thus make all the solution variables fairly comparable in magnitude. Our recommendations include scaling the equilibrium minority carrier density, p_{no}, by 10^{-2} and the diffusion lengths, L_p and L_{p_r}, by 10^4.

We also observe that the equations themselves are widely disparate in magnitude. We must therefore multiply the equations by the appropriate scaling factors. The first two equations in the system involve expressions of S_p over D_p. The order of magnitude of these expressions is then roughly between one and two. Using this scale for the remaining equations, we multiply the two expressions containing the saturation current densities by 10^{15} and the four expressions containing the decay rates by 10^{-4}. These scaling factors are reasonable considering that typical values of the saturation current densities and the decay rates are 1.0×10^{-13} amps–cm^{-2} and 1.0×10^{-5} to 1.0×10^{-4} sec, respectively.

With the proper scaling the system of equations becomes

$$\beta_J \cot \beta_J W = -\frac{S_p}{D_p} \tag{C.12}$$

$$\beta_V + \frac{S_p \beta_{V_r} \cot \beta_{V_r} W_r}{D_p \beta_V} = \frac{1}{\tan \beta_V W} \left[\frac{S_p}{D_p} - \beta_{V_r} \cot \beta_{V_r} W_r \right] \tag{C.13}$$

$$\frac{d}{\tau_J} = d \beta_J^2 D_p + \frac{d D_p}{\left(\hat{L}_p b \right)^2} \tag{C.14}$$

$$\frac{d}{\tau_V} = d\,\beta_V^2 D_p + \frac{d\,D_p}{\left(\hat{L}_p\,b\right)^2} \tag{C.15}$$

$$c\,J_o = -c\,q\,\hat{p}_{no}\,a\,D_p\,\beta_{V_r}\cot\beta_{V_r}W_r + c\,q\,\hat{p}_{no}\,a\,\frac{D_p}{\hat{L}_p\,b}\left[\frac{\frac{S_p\hat{L}_p\,b}{D_p} + \tanh\frac{W}{\hat{L}_p\,b}}{1 + \frac{S_p\hat{L}_p\,b}{D_p}\tanh\frac{W}{\hat{L}_p\,b}}\right] \tag{C.16}$$

$$\frac{d}{\tau_{J_r}} = d\left(\frac{\pi}{W_r}\right)^2 D_p + \frac{d\,D_p}{\left(\hat{L}_{p_r}\,b\right)^2} \tag{C.17}$$

$$\frac{d}{\tau_{V_r}} = d\,\beta_{V_r}^2 D_p + \frac{d\,D_p}{\left(\hat{L}_{p_r}\,b\right)^2} \tag{C.18}$$

$$c\,J_{o_r} = -c\,q\,\hat{p}_{no}\,a\,D_p\,\beta_{V_r}\cot\beta_{V_r}W_r + c\,q\,\hat{p}_{no}\,a\,\frac{D_p}{\hat{L}_{p_r}\,b}\coth\frac{W_r}{\hat{L}_{p_r}\,b} \tag{C.19}$$

where the scaling factors are

$$a = 1.0 \times 10^2$$

$$b = 1.0 \times 10^{-4}$$

$$c = 1.0 \times 10^{15}$$

$$d = 1.0 \times 10^{-4}$$

and the scaled versions of p_{no}, L_p, and L_{p_r} are indicated by $\hat{p}_{no}$, $\hat{L}_p$, and $\hat{L}_{p_r}$, respectively.

C.2 Conversion of Equations to Fortran

We are now ready to write the system of equations in Fortran in preparation for its solution by SECANT. SECANT requires that the entire system of equations be written into a subroutine called FCN, where F, X, and UDF are the calling variables. In FCN each independent solution variable of the system is renamed as a element in the array X(i), i=1,...,8. Also, each equation is set equal to zero and assigned an equation number F(i) such that the equations are in the form F(i) = 0, i=1,...,8. We note that it is possible to define permissible regions of solutions for each of the solution variables using UDF. We find this feature especially useful for the eigenvalues whose physically acceptable values are confined to particular regions as discussed in the section on singularities.

C.3 Call to SECANT

We initiate the solution by SECANT by writing the following statement in our Fortran program:

CALL SECANT(X, N, FCN, NDIGIT, RNORM).

X, we recall, is the solution vector. We must supply in X an initial guess to the solution. A suitable initial guess could be the typical values for the solution discussed in the section on scaling. Remembering to scale, the initial guess is then:

$$S_p = 300 \ \text{cm–sec}^{-1}$$

$$\hat{p}_{no} = 100 \ \text{cm}^{-3}$$

$$D_p = 10 \ \text{cm}^2\text{–sec}^{-1}$$

$$\beta_J = 50 \ \text{cm}^{-1}$$

$$\beta_V = 30 \ \text{cm}^{-1}$$

$$\beta_{V_r} = 30 \ \text{cm}^{-1}$$

$$\hat{L}_p = 500 \ \text{cm}$$

$$\hat{L}_{p_r} = 500 \ \text{cm}.$$

The best approximation to the roots of the system by SECANT is returned in X.

N represents the number of independent variables (and the number of equations) to be solved by SECANT. For our system, N equals eight.

FCN is the subroutine containing the system of simultaneous equations to be evaluated and has been described in the preceding section.

NDIGIT is the number of digit accuracy desired. We select NDIGIT to be seven.

RNORM is left as a variable. Upon entering SECANT, RNORM is set to specify the writing of the initial and final solution to an output file. Upon returning from SECANT, RNORM gives information on the relative convergence of the solution. The criterion for convergence of the solution is that the difference between components of two successive approximations be less than $10^{-NDIGIT}$. RNORM is defined as

$$RNORM = F(1)^2 + F(2)^2 + \cdots + F(8)^2. \qquad (C.20)$$

RNORM also will indicate when a convergent solution is not possible.

C.4 Program Listing

```
15154,mqe,cm60000,t25
mnf.
#eor
      program solve(input,output)
c          this program uses the library subroutine SECANT
c          to solve the system of eight simultaneous equations
c          comprising the Combined Model.


      dimension x(8), f(8)
      external  fcn
      common pi,q,tj,tv,xjtot,w,tjr,tvr,xjtotr,wr,xnd,a,b,c,d
c
c
c     physical constants
c
          pi = 3.1415927
          q  = 1.6e-19
c
c
c     measurements
c
c        bsf
c         tj      = short circuit current decay rate (sec)
c         tv      = open circuit voltage decay rate (sec)
c         xjtot   = total saturation current (amps per cm sq.)
c         w       = cell width (cm)
c
c        bsf removed
c         tjr     = short circuit current decay rate (sec)
c         tvr     = open circuit voltage decay rate (sec)
c         xjtotr  = total saturation current (amps per cm sq.)
c         wr      = cell width (cm)
c
c
          tj      =   42.1454 e-06
          tv      =   89.3249 e-06
          xjtot   =  390.2490 e-15
          w       =  533.0000 e-04
          tjr     =   24.3413 e-06
          tvr     =   54.4172 e-06
          xjtotr  =  462.5770 e-15
          wr      =  523.0000 e-04
c
c
c     empirical data
c
c         base doping (per cubic cm)
c
          xnd = 2.0e+16
c
c
c     print the input data
c
          print 100, tj,tv,xjtot,w,tjr,tvr,xjtotr,wr,xnd
  100     format(x,'measurements',//,
```

```
     +    5x,'tj    =',3x,e10.3,2x,'sec',/,
     +    5x,'tv    =',3x,e10.3,2x,'sec',/,
     +    5x,'jtot  =',3x,e10.3,2x,'amps per cm sq.',/,
     +    5x,'w     =',3x,e10.3,2x,'cm',/,
     +    5x,'tjr   =',3x,e10.3,2x,'sec',/,
     +    5x,'tvr   =',3x,e10.3,2x,'sec',/,
     +    5x,'jtotr =',3x,e10.3,2x,'amps per cm sq.',/,
     +    5x,'wr    =',3x,e10.3,2x,'cm',/,
     +    5x,'nd    =',3x,e10.3,2x,'per cubic cm',//)
c
c     scaling factors
c
          a = 1.0e+02
          b = 1.0e-04
          c = 1.0e+15
          d = 1.0e-04
c
c     identification of solution variables
c
c         x(1) = dp  = diffusion coefficient
c                      [cm sq. per sec]
c         x(2) = bvr = open circuit voltage decay eigenvalue (bsf removed)
c                      [per cm]
c         x(3) = bj  = short circuit current decay eigenvalue
c                      [per cm]
c         x(4) = sp  = back surface recombination velocity
c                      [cm per sec]
c         x(5) = bv  = open circuit voltage decay eigenvalue
c                      [per cm]
c         x(6) = pno = minority carrier concentration in the base
c                      [e+02 per cubic cm, scaled by a]
c         x(7) = lpr = diffusion length (bsf removed)
c                      [cm, scaled by b]
c         x(8) = lp  = diffusion length
c                      [cm, scaled by b]
c
c
c     initial guess at solution variable
c
          x(1) =   10.0
          x(2) =   30.0
          x(3) =   50.0
          x(4) =  500.0
          x(5) =   30.0
          x(6) =  100.0
          x(7) =  500.0
          x(8) =  500.0
c
c
c     call secant to solve the system of equations
c
c          the loop is set at four iterations in order to
c          allow the initial guess to be updated
c
c          rnorm greater than zero indicates that convergence
c          has been reached
```

```
c
                do 400 j=1,4
                rnorm = 2.0
                call secant(x,8,fcn,12,rnorm)
                if (rnorm.gt.0)  go to 499
  400           continue
c
c
c     compute the dependent solutions
c
c          xni  =  intrinsic carrier concentration
c          xjeo =  emitter component of the saturation current
c          xjbo =  base component of the saturation current
c          tp   =  minority carrier lifetime in the base
c          tpr  =  minority carrier lifetime in the base (bsf removed)
c
  499       xni   = sqrt(x(6)*a*xnd)
            xjeo  = - q*x(6)*a*x(1)*x(2)/tan(x(2)*wr)
            xbase = xjtot - xjeo
            tp    = ((x(8)*b)**2)/x(1)
            tpr   = ((x(7)*b)**2)/x(1)
c
c
c     print the solutions (independent and dependent)
c
            print 200, x(1),x(2),x(3),x(4),x(5),x(6),x(7),x(8),
     +                 xni,xjeo,xbase,tp,tpr
  200       format(///,'solutions',//,
     +      5x,'dp  =',3x,f10.3,3x,'cm sq per sec',/,
     +      5x,'bvr =',3x,f10.3,3x,'per cm',/,
     +      5x,'bj  =',3x,f10.3,3x,'per cm',/,
     +      5x,'sp  =',3x,f10.3,3x,'cm per sec',/,
     +      5x,'bvr =',3x,f10.3,3x,'per cm.',/,
     +      5x,'pno =',3x,f10.3,3x,'e+02 per cubic cm',/,
     +      5x,'lpr =',3x,f10.3,3x,'um',/,
     +      5x,'lp  =',3x,f10.3,3x,'um',/,/,
     +      5x,'ni  =',3x,e15.3,3x,'per cubic cm',/,
     +      5x,'jeo =',3x,e15.3,3x,'amps per cm sq.',/,
     +      5x,'jbo =',3x,e15.3,3x,'amps per cm sq.',/,
     +      5x,'tp  =',3x,e15.3,3x,'sec',/,
     +      5x,'tpr =',3x,e15.3,3x,'sec')
            stop
            end
c
c
c     subroutine containing the system of equations comprising
c         the Combined Model
c
            subroutine fcn(x,f,udf)
c               (the udf feature is not used)
            dimension x(8), f(8)
            common pi,q,tj,tv,xjtot,w,tjr,tvr,xjtotr,wr,xnd,a,b,c,d
c
            f(1) = x(3)/tan(x(3)*w) + x(4)/x(1)
            f(2) = (x(5)+(x(4)*x(2)*(1.0/tan(x(2)*wr)))/(x(1)*x(5)))
     +             - (1/tan(x(5)*w)*(x(4)/x(1) - x(2)/(tan(x(2)*wr))))
```

```
      f(3) = d/tj - d*(x(3)**2)*x(1) - d*x(1)/((x(8)*b)**2)
      f(4) = d/tv - d*(x(5)**2)*x(1) - d*x(1)/((x(8)*b)**2)
      f(5) = c*xjtot + c*q*x(6)*a*x(1)*x(2)*(1.0/tan(x(2)*wr))
     +          - c*q*x(6)*a*(x(1)/(x(8)*b))*
     +            (x(4)*(x(8)*b/x(1)) + tanh(w/(x(8)*b)))/
     +            (1.0 + x(4)*(x(8)*b/x(1))*
     +            tanh(w/(x(8)*b)))
      f(6) = d/tjr - d*((pi/wr)**2)*x(1) - d*x(1)/((x(7)*b)**2)
      f(7) = d/tvr - d*(x(2)**2)*x(1) - d*x(1)/((x(7)*b)**2)
      f(8) = c*xjtotr + c*q*x(6)*a*x(1)*x(2)*(1.0/tan(x(2)*wr))
     +          - c*q*x(6)*a*(x(1)/(x(7)*b))*
     +            (1.0/tanh(wr/(x(7)*b)))
      return
      end
c
c
#eor
#eof
```